The three-dimensional nature of boundary-layer instability

By P. S. KLEBANOFF, K. D. TIDSTROM AND L. M. SARGENT
National Bureau of Standards, Washington, D.C.

(Received 5 June 1961)

An experimental investigation is described in which principal emphasis is given to revealing the nature of the motions in the non-linear range of boundary-layer instability and the onset of turbulence. It has as its central purpose the evaluation of existing theoretical considerations and the provision of a sound physical model which can be taken as a basis for a theoretical approach. The experimental method consisted of introducing, in a two-dimensional boundary layer on a flat plate at 'incompressible' speeds, three-dimensional disturbances under controlled conditions using the vibrating-ribbon technique, and studying their growth and evolution using hot-wire methods. It has been definitely established that longitudinal vortices are associated with the non-linear three-dimensional wave motions. Sufficient data were obtained for an evaluation of existing theoretical approaches. Those which have been considered are the generation of higher harmonics, the interaction of the mean flow and the Reynold stress, the concave streamline curvature associated with the wave motion, the vortex loop and the non-linear effect of a three-dimensional perturbation. It appears that except for the latter they do not adequately describe the observed phenomena. It is not that they are incorrect or may not play a role in some aspect of the local behaviour, but from the over-all point of view the results suggest that it is the non-linear effect of a three-dimensional perturbation which dominates the behaviour. A principal conclusion to be drawn is that a new perspective, one that takes three-dimensionality into account, is required in connexion with boundary-layer instability. It is demonstrated that the actual breakdown of the wave motion into turbulence is a consequence of a new instability which arises in the aforementioned three-dimensional wave motion. This instability involves the generation of 'hairpin' eddies and is remarkably similar in behaviour to 'inflexional' instability. It is also shown that the results obtained from the study of controlled disturbances are equally applicable to 'natural' transition.

1. Introduction

One of the most important problems in fluid mechanics which has attracted the interest of investigators for many years is that of the transition from laminar to turbulent flow. The particular case of boundary-layer flow has received the most attention and has been more successfully treated than any other. However, despite the success of the linearized theories in revealing the nature of the initial stages of boundary-layer instability, there remains a deep void in the under-

standing of the subsequent non-linear behaviour and the actual breakdown of the laminar boundary layer. The present state of affairs is such that one must depend on experiment to bridge the gap. Much of the recent experimental activity has been in supersonic flows where the experimental techniques are somewhat limited. The possibilities of hot-wire techniques, which have been so successful in subsonic flows, have yet to be demonstrated for supersonic flows; and use has been made primarily of optical methods which for the most part reveal only the grosser aspects of the phenomenon. Consequently, much of the experimental activity dealing with boundary-layer transition in high-speed flows has consisted of varying parameters over wide limits and observing where transition occurs. Although a practical necessity, this type of approach at best reflects only indirectly the mechanism of transition and adds little to an understanding of the fundamental mechanism. Although the bulk of present-day interest is in the supersonic and hypersonic flow régimes, the low-speed régime still provides the best experimental conditions for examining the mechanics of transition, principally because the hot-wire anemometer can be used to good advantage and boundary layers are thicker.

A long-range investigation into the mechanics of transition, combining a low-speed and a supersonic-speed programme, has been undertaken at the National Bureau of Standards under the sponsorship of the National Aeronautics and Space Administration. The low-speed phase of the programme, with which the present paper is concerned, is directed toward obtaining an insight into the fundamental processes governing transition, and providing a basis for comparison and evaluation of the work done at supersonic speeds. Recent accounts of progress made to date were given by Klebanoff & Tidstrom (1959) and Spangenberg & Rowland (1960).

The work of Schubauer & Klebanoff (1956) showed transition to be a process involving the formation of turbulent spots, as had been postulated earlier by Emmons (1951). However, the manner in which a turbulent spot arises from growing perturbations in the boundary layer remained an open question. Schubauer (1957) and Klebanoff & Tidstrom (1959) pointed out that there is a definite and reproducible progression of events by which Tollmien–Schlichting waves evolve into turbulence. This evolution comprises three stages of development: a primary stage which is governed by the two-dimensional linearized stability theories, a second stage of finite amplitude where strong three-dimensional effects are observed, and a third stage involving the birth of turbulent spots. The primary stage is fairly well understood, and the present investigation has been directed toward a more thorough understanding of the latter two stages. Much of the theoretical effort dealing with the region of finite amplitude has in the past centred on the two-dimensional approach. However, in recent years there has been an increased awareness of the three-dimensionality associated with boundary-layer instability. Apart from the aforementioned references, the experimental investigations of Hama, Long & Hegarty (1957), Fales (1955), and Weske (1957) utilizing dye techniques in water have demonstrated the occurrence of characteristic three-dimensional dye configurations before transition occurs. In addition, the theoretical investigations of Theodorsen (1955), Görtler & Wit-

ting (1957), and more recently Benney & Lin (1960), have also dealt with various aspects of the three-dimensionality. None of the considerations of either the two-dimensional or three-dimensional approaches is necessarily mutually exclusive, and it becomes one of the prime objectives of experiment to determine their relative significance and to point out the nature of the principal non-linear mechanism. This investigation therefore has as its central purpose the evaluation of existing theoretical considerations with the goal of providing a sound physical model as a basis for theory.

2. Experimental procedure

In this investigation the growth and evolution of disturbances are studied under controlled conditions using the vibrating-ribbon technique developed by Schubauer & Skramstad (1948) for the introduction of forced oscillations. The experimental arrangement is essentially the same as that described in detail by Klebanoff & Tidstrom (1959). Briefly stated, the investigation was conducted on an aluminium flat plate, 12 ft. long, 4·5 ft. wide and 0·25 in. thick, with a symmetrically tapered and sharpened leading edge. The plate was mounted vertically and centrally in the Bureau of Standards' 4·5 ft. wind tunnel. The pressure gradient was adjustable within moderate limits and was adjusted to give zero pressure gradient along the plate. The ribbon of brass 0·002 in. thick, 0·18 in. wide, and 36 in. long was transverse to the flow at 0·009 in. from the surface and 35 in. from the leading edge. The middle segment, 13 in. long, was free to vibrate when driven by means of an alternating current of the desired frequency in the presence of a steady magnetic field.

The study of the three-dimensional effects associated with the wave motions which was described by Schubauer (1957) and Klebanoff & Tidstrom (1959) was complicated by small pre-existing mean-flow variations in the spanwise direction which were introduced from the free stream. The inference drawn from this earlier work was that the initial effect of the mean-flow variations was to make the wave three-dimensional, and that the three-dimensional wave motions would then generate longitudinal vortices. However, the pre-existing mean-flow irregularities tended to obscure this effect. These irregularities were removed by installing new damping screens in the wind tunnel, and a uniform mean flow with barely detectable variations was obtained. Nevertheless, the same general behaviour was observed, namely the development of a three-dimensionality characterized by spanwise variations in wave amplitude. It appeared, therefore, that the development of this three-dimensional pattern was an inherent phenomenon constituting an important aspect of boundary-layer instability. Consequently it was decided to control the spanwise variation in wave amplitude in order that the structure and significance of the observed three-dimensionality could be reliably studied in detail. This was done by placing single strips of cellophane tape (0·003 in. thick), 0·5 in. long and 0·5 in. apart, on the surface beneath the vibrating ribbon.

Figure 1 shows the spanwise distribution of mean velocity obtained with this experimental arrangement. The measurements were made at a fixed distance

from the surface, $y = 0{\cdot}042$ in., and at different distances x_1 downstream from the vibrating ribbon; z represents the distance in the spanwise direction, and $z = 0$ corresponds to the centre-line of the plate. The velocity is plotted as the ratio U/U_1, where U is the longitudinal component of local mean velocity within the boundary layer and U_1 is the free-stream velocity. At 7 in. downstream from the ribbon, the measurements made with the ribbon and spacers in place (ribbon not vibrating) are compared with those obtained with the ribbon and spacers

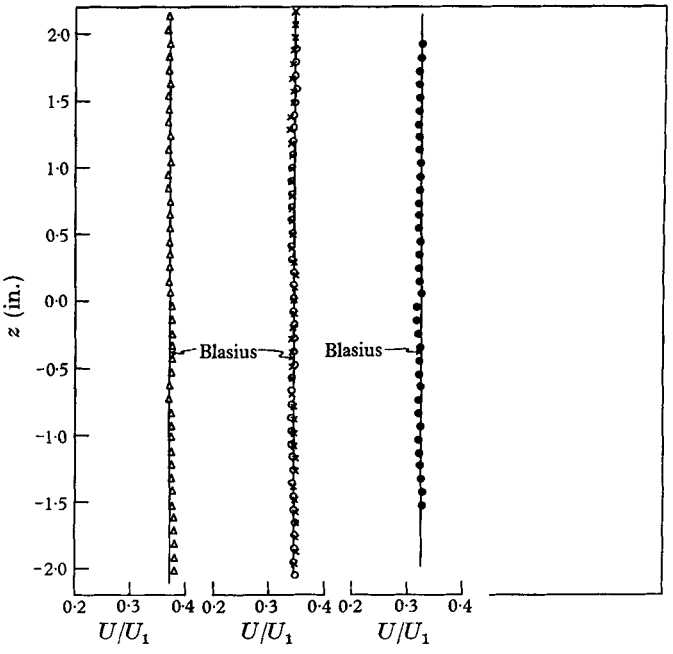

FIGURE 1. Spanwise distribution of mean velocity at different distances downstream from vibrating ribbon: $y = 0{\cdot}042$ in., $U_1/\nu = 3{\cdot}1 \times 10^5$ ft.$^{-1}$. Ribbon and spacers: △, $x_1 = 1$ in.; ○, $x_1 = 7$ in.; ●, $x_1 = 10$ in. No ribbon and spacers: ×, $x_1 = 7$ in.

removed. It is seen that these devices have introduced no noticeable distortion in the mean flow. Except for observed variations on the order of 1 %, which are within the experimental uncertainty, the mean flow is closely two-dimensional and in good agreement with the Blasius value. The boundary-layer thickness is approximately 0·2 in., and a variation of 0·001 in. from the surface would give a $2\frac{1}{2}$ % change in velocity. Consequently any spanwise irregularities which may still exist in the mean flow would be quite small and hidden by the experimental uncertainty.

The hot-wire techniques used are dealt with in the literature so extensively that they need not be described here. Platinum wires 0·0001 in. in diameter and ranging in length from 0·5 to 1·0 mm were used. Detailed surveys were made of the longitudinal and spanwise component of mean velocity, as well as of the mean-square and instantaneous values of the longitudinal and spanwise fluctuations. Measurements of the spanwise component which involves the use of two wires were made using a V-wire arrangement, rather than the customary X-type, in

order to avoid difficulty from the steep gradients across the layer. The separation between centres of the wires in the V-wire arrangement was 0·5 mm. No hot-wire length corrections were applied to any of the data; nor, except where specifically stated, was a correction made for the non-linearity of the hot-wire. Film recordings of the fluctuations from a dual-beam cathode-ray oscilloscope also proved extremely useful. The shutter speed of the camera was somewhat slower than the sweep speed, and consequently an overlay of the trace was observed in some of the oscillograms in which the trace was not exactly repetitive.

For the most part, the data presented were obtained with a 145 c/s wave and at a free-stream speed of about 50 ft./sec. The speed was changed within moderate limits to keep a constant Reynolds number per foot of $3{\cdot}1 \times 10^5$. At this Reynolds number per foot, natural transition occurred at about 9 ft. from the leading edge. The boundary-layer Reynolds number based on displacement thickness at the vibrating ribbon position was 1635, which placed the 145 c/s wave near branch II of the Tollmien–Schlichting stability diagram.

3. Nature of wave

Figure 2 shows the spanwise distribution of intensity for a 145 c/s zone at 0·042 in. from the surface, and at 3, 6, and 7·5 in. downstream from the vibrating ribbon. This y-position was chosen because it was about the position where the maximum in the Tollmien–Schlichting distribution of wave amplitude occurred. Here u' is the root-mean-square value of the longitudinal fluctuation u. The distributions shown were obtained with a fixed amplitude of the vibrating ribbon. They demonstrate the well-controlled three-dimensionality of the wave as evidenced by the uniformly large differences in intensity between peaks and valleys. The spanwise wavelength is 1 in., and the location of the spacers beneath the vibrating ribbon in relation to the spanwise variation in intensity is also noted in the figure. The peaks and valleys maintain a fixed spanwise position as they intensify in the downstream direction. Breakdown of the wave has not yet occurred for the distributions shown.

In figure 3 the growth in wave intensity is shown for two different amplitudes of the vibrating ribbon; x is the distance in the downstream direction as measured from the leading edge of the flat plate. The measurements were made along lines corresponding to a peak and a neighbouring valley at 0·045 in. from the surface. The intensity is plotted relative to u'_0, which is the intensity at a reference position x_0, 3 in. downstream from the vibrating ribbon. The low-amplitude wave which amplifies and then damps obeys linear theory. It shows the same behaviour at the different spanwise positions and has a neutral position and wave velocity which are in good agreement with the theory. At the higher amplitude the wave at peak and valley at first follows the rate of growth as given by linear theory, and then exhibits the characteristically different behaviour associated with the region of finite amplitude, namely a very rapid growth at the peak and an initial growth at the valley less than that of the linear theory. Increasing the ribbon amplitude had no significant effect on the character of the wave generated

except to move the point of departure and breakdown further upstream. With sufficiently large amplitude it was possible to by-pass the linear range completely. This was graphically demonstrated by observing the behaviour of a wave of

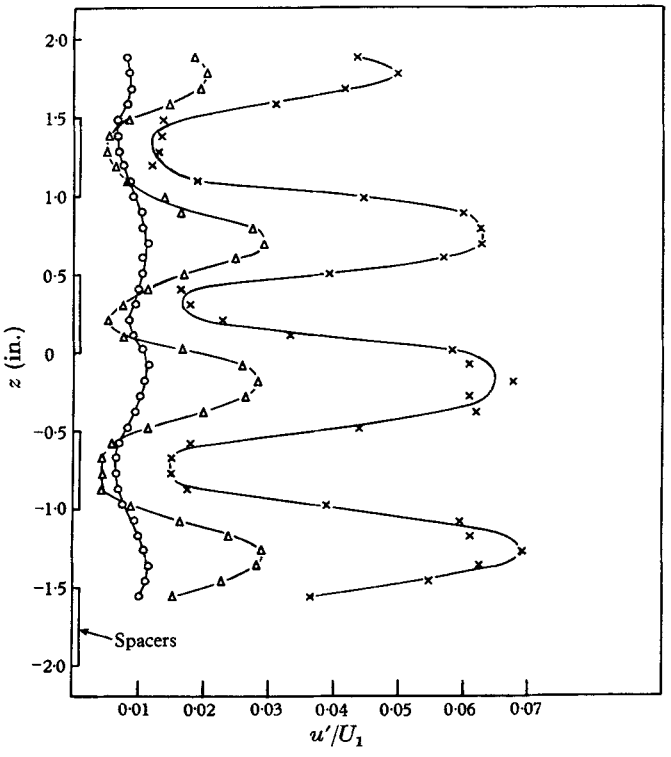

FIGURE 2. Spanwise distributions of intensity of u-fluctuation at different distances downstream from vibrating ribbon: 145 c/s wave, $y = 0{\cdot}042$ in., $U_1/\nu = 3{\cdot}1 \times 10^5$ ft.$^{-1}$. ○, $x_1 = 3$ in.; △, $x_1 = 6$ in.; ×, $x_1 = 7{\cdot}5$ in.

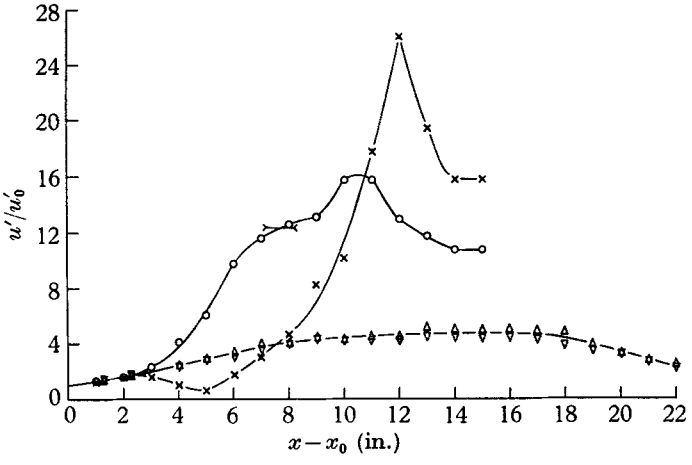

FIGURE 3. Wave growth at peak and valley: 145 c/s wave, $y = 0{\cdot}045$ in., $U_1/\nu = 3{\cdot}1 \times 10^5$ ft.$^{-1}$. Peak: △, $u_0'/U_1 = 0{\cdot}0008$; ○, $u_0'/U_1 = 0{\cdot}007$. Valley: ▽, $u_0'/U_1 = 0{\cdot}0007$; × $u_0'/U_1 = 0{\cdot}005$. >—<, Breakdown.

such frequency that it should damp according to the linear theory. At low amplitudes the wave damped as expected, but at a sufficiently high amplitude it did not damp and very rapidly led to breakdown of laminar flow in much the same manner as a wave within the amplified zone. The breakdown process is described in § 5. After breakdown, which occurs only at a peak, the intensity at both peak and valley continues to increase to a maximum and then subsides to the turbulent flow condition. In figure 4 the data for the higher amplitude wave of figure 3 is replotted to illustrate the actual intensities involved. The

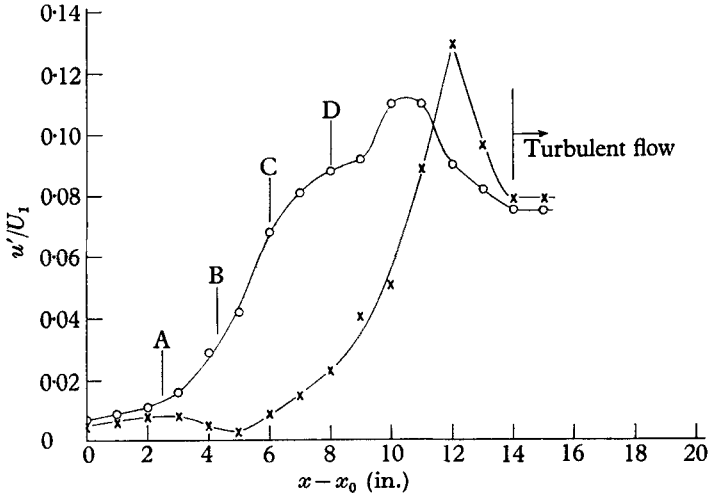

FIGURE 4. Intensity of u-fluctuation at peak and valley for the higher amplitude wave of figure 3. ○, $z = -0{\cdot}2$ in. (peak); ×, $z = -0{\cdot}75$ in. (valley).

stations A, B, C, and D noted in the figure are the different downstream positions at which detailed observations were made, with station A corresponding to the position of departure from the linear theory and station D to the position of breakdown. It is the region from departure to breakdown, and the region from breakdown to fully developed turbulent flow which are of principal interest.

A more detailed picture of the spanwise variation in wave intensity, as well as the rate of growth, is shown in figure 5, where the intensity distribution across the boundary layer for different spanwise positions from a peak to a valley are compared on a non-dimensional basis at the downstream positions A, B, C and D. The non-dimensional distance y/δ is used, where δ is the boundary-layer thickness given by

$$\delta = 5{\cdot}0\sqrt{(\nu x/U_1)}.$$

It is evident that the spanwise variation as well as the wave growth depends markedly on distance from the surface. At the beginning of the non-linear range (station A) there is a relatively small spanwise variation in intensity, from $0{\cdot}05\delta$ to $0{\cdot}3\delta$. This variation is in the vicinity of the critical layer, which is a region near $0{\cdot}2\delta$ where the wave velocity is equal to the mean velocity, and is indicative of the 'weakness' of the critical layer in the instability process (see Benney & Lin 1960). The differences between peak and valley increase in magnitude and extend over more and more of the boundary layer as breakdown is approached.

In contrast to the intensity distribution in the region of the valley, the intensity at a peak increases very rapidly from a maximum value of 1·3 % at station A to a maximum value of about 16 % at station D. The position of the maximum in the intensity distribution as given by linear theory is at $0{\cdot}2\delta$, but in the non-linear range the position of the maximum at a spanwise position corresponding to a peak moves away from the surface as breakdown is approached, and at breakdown has moved out to about $0{\cdot}4\delta$. Accompanying these differences in intensity there are also marked changes in the wave form at peak and valley. These are

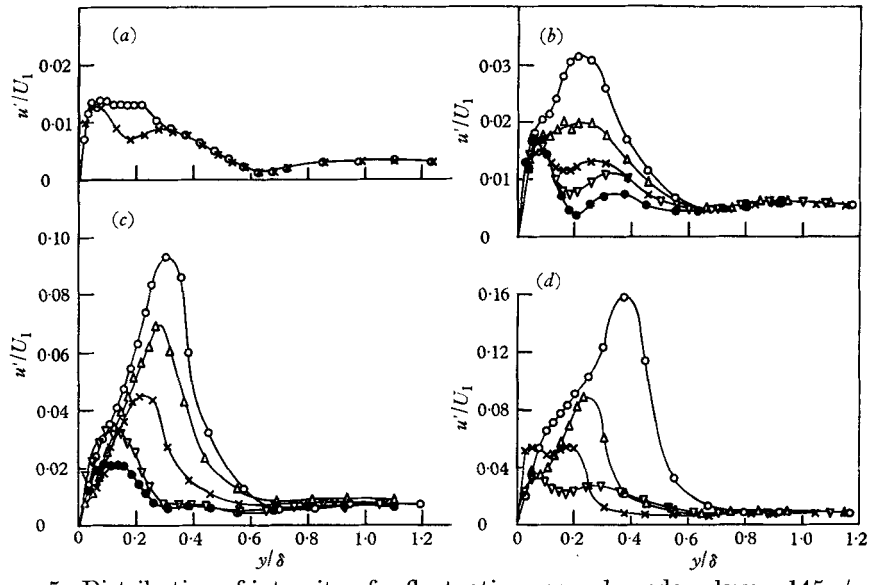

FIGURE 5. Distribution of intensity of u-fluctuation across boundary layer: 145 c/s wave, $U_1/\nu = 3{\cdot}1 \times 10^5$ ft.$^{-1}$. (*a*) Station A: ○, $z = -0{\cdot}2$ in.; ×, z, $= -0{\cdot}75$ in. (*b*) Station B: ○, $z = -0{\cdot}2$ in.; △, $z = -0{\cdot}35$ in.; ×, $z = -0{\cdot}45$ in.; ▽, $z = -0{\cdot}55$ in.; ●, $z = -0{\cdot}65$ in. (*c*) Station C: ○, $z = -0{\cdot}2$ in.; △, $z = -0{\cdot}35$ in.; ×, $z = -0{\cdot}45$ in.; ▽, $z = -0{\cdot}55$ in.; ●, $z = -0{\cdot}65$ in. (*d*) Station D: ○, $z = -0{\cdot}2$ in.; △, $z = -0{\cdot}4$ in.; ×, $z = -0{\cdot}45$ in.; ▽, $z = -0{\cdot}55$ in.

illustrated by the oscillograms of figure 6, plate 1, in which the wave form of the u-fluctuation at a peak and valley are compared. The comparison is made for the 145 c/s wave which has the growth curve shown in figure 4. The observations were made at the different positions along the growth curve which are noted above each oscillogram, and at 0·045 in. from the surface. The reference signal referred to in the figure was the input signal to the vibrating ribbon. The reference signal and the fluctuation at a peak or a valley were observed simultaneously on a dual-beam cathode-ray oscilloscope. At $x - x_0 = 3{\cdot}0$ in., which is about the beginning of the non-linear range, the fluctuations at both peak and valley are free of visible distortion. They are in phase not only for the y-position shown but across the layer as well, and the wave front may still be considered two-dimensional. However, well within the non-linear range the behaviour is markedly different. The fluctuation at the peak remains relatively free of distortion, while that at the valley undergoes considerable distortion and exhibits a tendency to double

in frequency. The degree of distortion not only varies in the spanwise direction but also depends on distance from the surface. For example, the trace in the outer region of the layer is quite regular and in phase with that at the peak. This behaviour is a characteristic feature of the non-linear range and was observed to occur over a wide range of frequencies and Reynolds number per foot.

Measurements of the phase of the u-fluctuation at a spanwise position corresponding to a peak, which are shown in figures 7 and 8, illustrate that the wave motion, despite the aforementioned complexities, still retains some semblance of linear behaviour. Such measurements were not feasible in the region of the

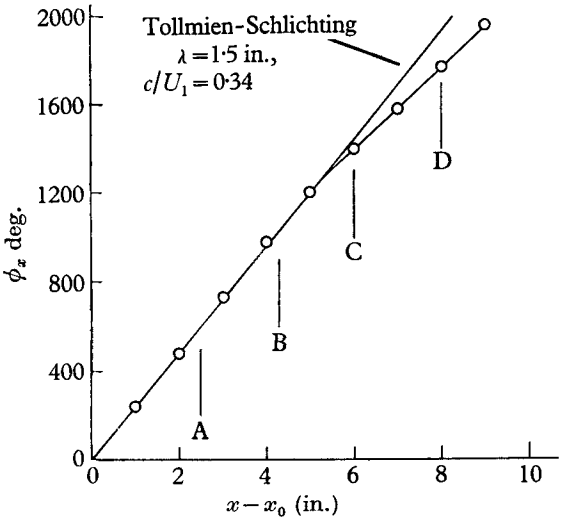

FIGURE 7. Phase of u-fluctuation in downstream direction: 145 c/s wave, $y = 0{\cdot}045$ in., $U_1/\nu = 3{\cdot}1 \times 10^5$ ft.$^{-1}$.

valley because of the wave distortion. In figure 7 the phase angle in the downstream direction, ϕ_x, was obtained from observations, such as shown in figure 6, plate 1, of the change in phase of the hot-wire signal with respect to the input signal to the vibrating ribbon as the distance downstream from the ribbon was varied. There is no significant departure of wave velocity and wavelength from that of the linear theory until just before breakdown. The wave velocity, $c = 0{\cdot}34U_1$, and the wavelength, $\lambda = 1{\cdot}5$ in., are still in excellent agreement with the Tollmien–Schlichting theory at station C. In the relatively short distance from station C to station D, a significant increase in wave velocity occurs with a corresponding increase in wavelength to about 2·0 in. The distribution of phase across the boundary layer at various stages of the downstream development is shown in figure 8. The phase angle ϕ_y is the change in phase relative to that observed at the outer edge of the layer, with an increasing angle indicating an advance in phase. The observations were made in much the same manner as for the downstream phase angle. At the beginning of the non-linear range there is the familiar phase shift associated with the linear theory. Although noticeable changes in magnitude as well as in the form of the distribution occur in the non-linear range, they may be regarded as not being substantial changes. The two distributions at station C

show the shift in phase in one case for the maximum in the velocity fluctuation and in the other for the minimum in the velocity fluctuation. Oscillograms illustrating the behaviour of the u-fluctuation at station C are shown in figure 14, plate 2. Within the experimental accuracy these distortions were not observed at stations A or B. A reasonable inference from the phase distributions at station C is that, associated with the increase in wave velocity as breakdown is approached, the crest of the three-dimensional wave tends to be displaced in the downstream direction. It may be that the distance from crest to crest of the wave may be slightly larger at breakdown than the 2·0 in. inferred from figure 7. The phase change across the boundary layer may become more pronounced as breakdown is approached, and since the measurements in figure 7 were made at only one y-position they do not necessarily reflect the true distance from crest to crest.

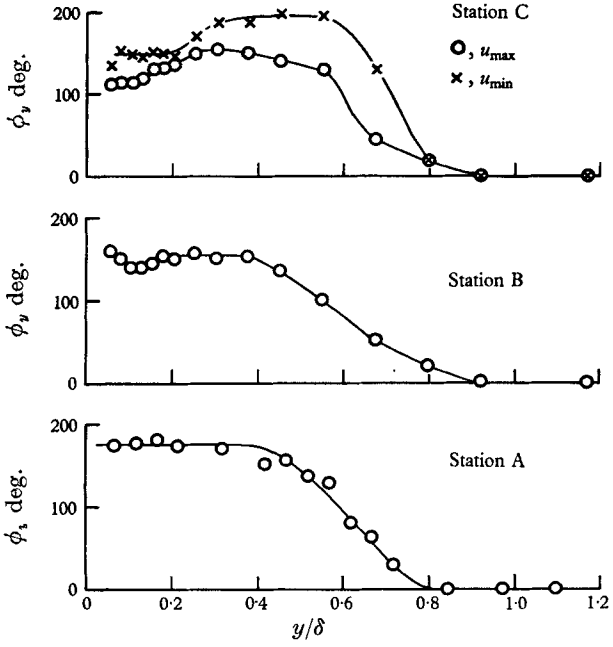

FIGURE 8. Phase of u-fluctuation across boundary layer: 145 c/s wave, $U_1/\nu = 3{\cdot}1 \times 10^5$ ft.$^{-1}$.

4. Experimental results and relation to theory

4.1. *Harmonics and Reynolds stresses*

It is evident from the wave behaviour just outlined that a purely two-dimensional approach is not sufficient for an adequate understanding of the non-linear range. However, in a general three-dimensional analysis, two-dimensional effects would still be included, and it is necessary that their importance be evaluated. The two-dimensional approach has in general centred on two effects, one dealing with the generation of higher harmonics, and the other the interaction between the Reynolds stress and the mean flow. According to an order-of-magnitude analysis of these two effects by Lin (1957), one would expect the non-linear behaviour to manifest itself, with increasing wave amplitude, in the generation of higher

harmonics in the vicinity of the critical layer before the distortion of the mean flow due to the Reynolds stress is observed. Measurements of the harmonic content in the vicinity of the critical layer associated with the wave growth at a spanwise position corresponding to a peak are shown in figure 9. The position of the critical layer becomes somewhat less well defined in the non-linear range, and its position referred to herein is that in the linear range. It is seen that the harmonic content

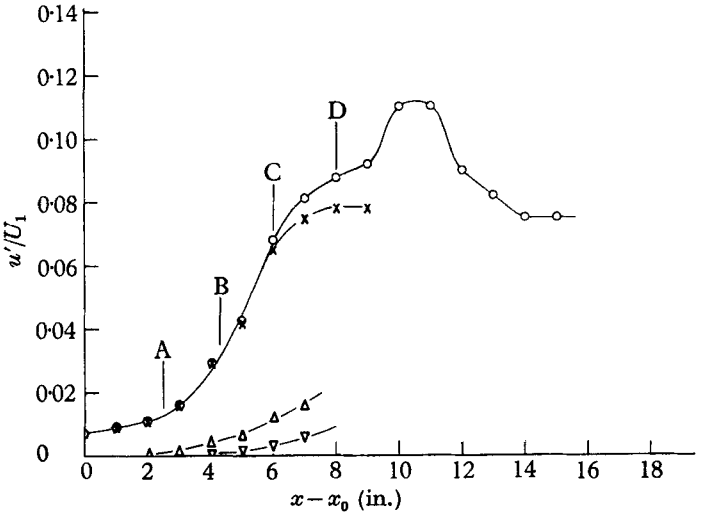

FIGURE 9. Harmonic content of u-fluctuation: 145 c/s wave, $y = 0{\cdot}045$ in., $U_1/\nu = 3{\cdot}1 \times 10^5$ ft.$^{-1}$.
○, total; ×, first harmonic; △, second harmonic; ▽, third harmonic.

is not what would be expected from the order-of-magnitude analysis. Just before departure from the linear theory, the intensity of the second harmonic is about 5 % of the fundamental. Contrary to the order-of-magnitude analysis, the harmonic content increases relatively slowly, and as breakdown is approached the intensity of the second harmonic is about 20 % and the third harmonic about 8 % of the fundamental. Within the experimental error the comparison of the over-all intensity with that of the first harmonic does not reflect the presence of the second and third harmonics until breakdown is approached. This is because measurement of the over-all intensity involves the sum of the squares of the various harmonics. It should also be pointed out that the effect of the non-linearity of the hot-wire is such that it would tend to contribute to the measured harmonic content. Measurements in the outer region of the boundary layer at about $0{\cdot}6\delta$ demonstrated that the harmonic content is of the same order as the harmonic content in the vicinity of the critical layer, and at breakdown is even larger. This is also contrary to the order-of-magnitude analysis.

The distribution of mean velocity across the boundary layer at a peak and valley, and at various stages of the wave development, are shown in figure 10. At station A the distributions at peak and valley are in excellent agreement with the Blasius distribution. As the wave grows, a significant change in the velocity profile takes place. At a peak the profile has developed a point of inflexion, and

exhibits a progressively greater defect in velocity as breakdown is approached. At a valley the profile tends to become fuller than the Blasius profile. These changes in the velocity profile are already noticeable at station B, soon after departure from the linear theory. Consequently there is no real evidence of any strong harmonic content occurring before distortion of the mean flow. It is also difficult to associate the observed changes in velocity profile with the Reynolds-stress mean-flow interaction treated by Meksyn & Stuart (1951) and Stuart

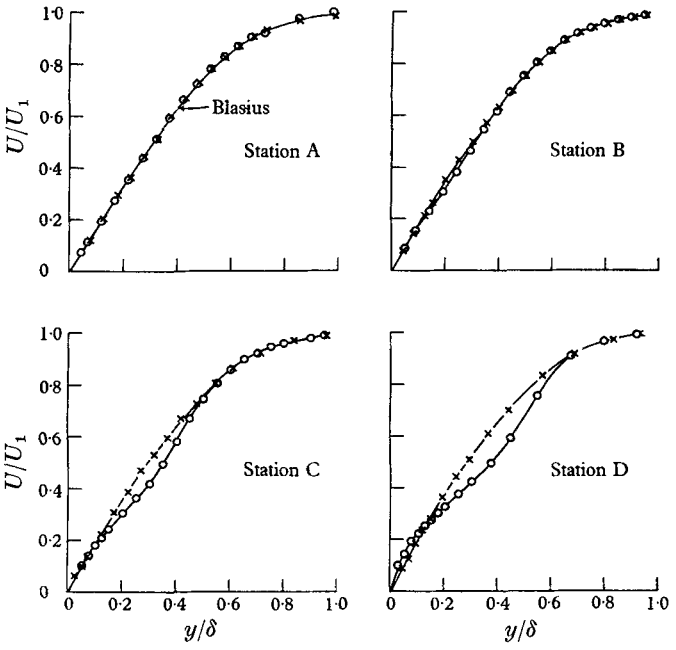

FIGURE 10. Mean velocity distributions across boundary layer at peak and valley: 145 c/s wave, $U_1/\nu = 3{\cdot}1 \times 10^5$ ft.$^{-1}$. ○, $z = -0{\cdot}2$ in.; ×, $z = -0{\cdot}75$ in.

(1958), inasmuch as the changes in profile at peak and valley are in the opposite direction. From these observations it is concluded that another mechanism comes into play and dominates the transition process to such an extent that higher-harmonic and Reynolds-stress effects become relatively insignificant amongst the various possible non-linear effects.

4.2. *Phenomena associated with three-dimensionality*

It is apparent that the changes in velocity profile are likely to be those associated with the superposition of a longitudinal eddy system. Figure 11 shows the spanwise distributions of the intensities of the longitudinal and spanwise fluctuations, as well as the spanwise distributions of the longitudinal and spanwise components of mean velocity; w' and W are the root-mean-square value of the spanwise fluctuation and the spanwise component of mean velocity, respectively. The measurements shown by the open-circle symbols were made at $0{\cdot}31\delta$ from the surface. Measurements of the spanwise component of mean velocity were also made at $0{\cdot}11\delta$, and these are shown by the dashed curve. Although the various

distributions shown were obtained at slightly different stages of the wave growth, in general they correspond rather closely to those at station C. The measurements of the spanwise component of mean velocity are perhaps the most interesting. They exhibit a maximum at each side of the peak in u', and a change in sign from one side to the other, as well as a change in sign across the boundary layer. A positive sign of W indicates that the flow direction is to the left as one views

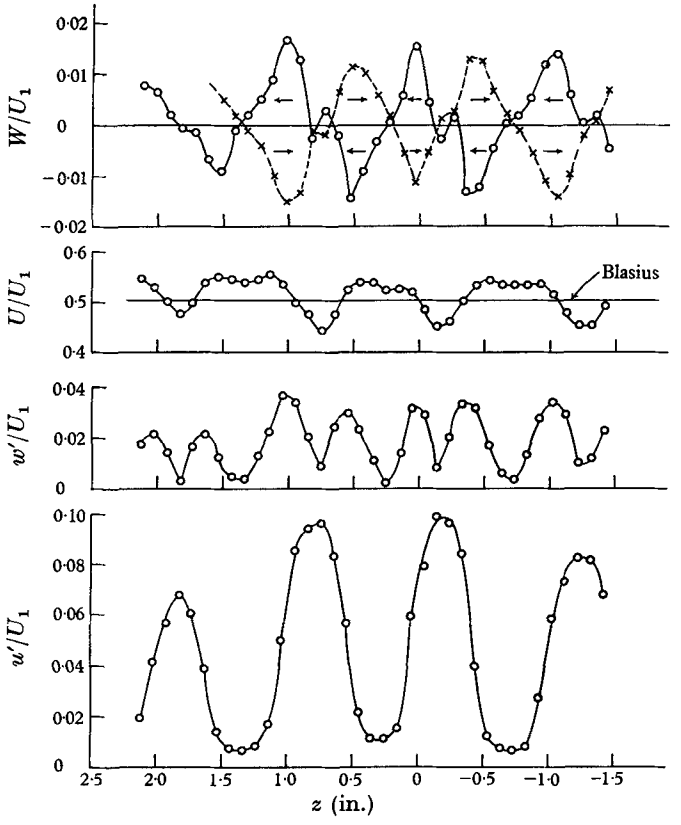

FIGURE 11. Spanwise distributions of mean and fluctuating components of velocity: 145 c/s wave, $U_1/\nu = 3{\cdot}1 \times 10^5$ ft.$^{-1}$. ——, $y = 0{\cdot}31\delta$; – – – –, $y = 0{\cdot}11\delta$.

the figure. However, since the measurements indicated by the dashed curve were obtained closer to the surface, the arrows indicating flow direction were arbitrarily changed in the region on the right side of the peak in u' to illustrate that, in the spatial configuration, the eddies are rotating in a clockwise direction on one side of the peak and in a counterclockwise direction on the other side. The distribution of mean velocity is found to be distorted in the manner expected from the superposition of a longitudinal eddy system rotating as shown. The intensity of the spanwise fluctuation has, as would also be expected, a maximum on each side of the peak in u' and therefore exhibits half the wavelength. Figure 12 shows the distribution of W across the boundary layer at each side of a peak in u' (where w' is a maximum) at stations B and C. It is seen that associated with the wave growth there is a strong intensification of the eddy system, accompanied

by an increase in the extent of the eddy across the boundary layer, as breakdown is approached.

A plausible explanation for the effect of the spacers beneath the vibrating ribbon in inducing a spanwise variation in wave amplitude is that they give rise

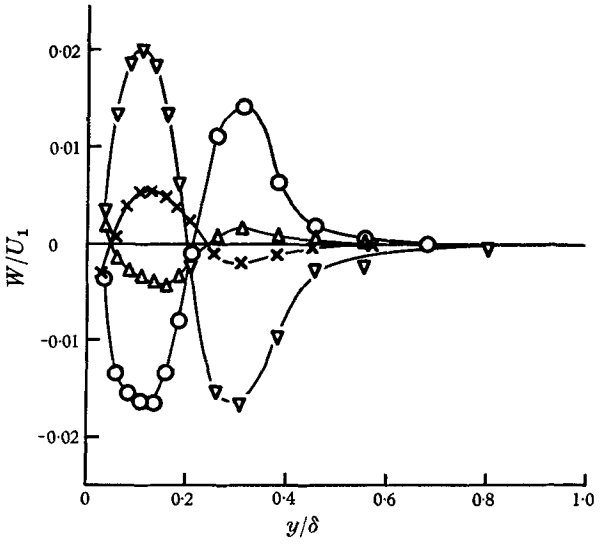

FIGURE 12. Distributions of spanwise component of mean velocity across boundary layer. 145 c/s wave, $U_1/\nu = 3{\cdot}1 \times 10^5$ ft.$^{-1}$. Station B: △, $z = 0{\cdot}0$ in.; ×, $z = 0{\cdot}4$ in. Station C: ○, $z = 0{\cdot}0$ in.; ▽, $z = -0{\cdot}4$ in.

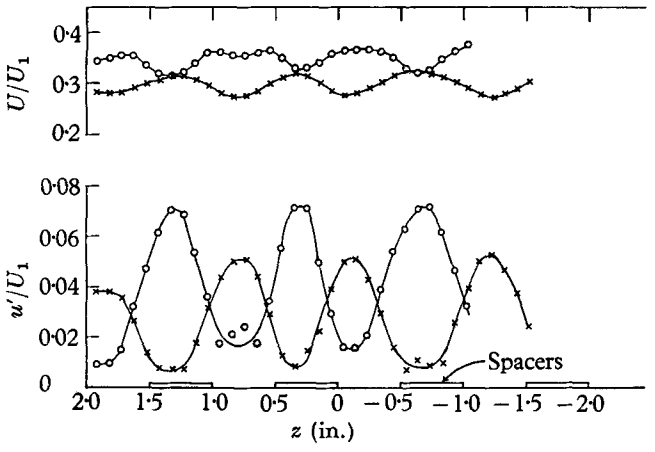

FIGURE 13. Spanwise distribution of mean velocity and intensity of u-fluctuation at two different Reynolds numbers per foot: 65 c/s wave, $x = 3{\cdot}75$ ft. ○, $U_1/\nu = 3{\cdot}1 \times 10^5$, $y = 0{\cdot}043$ in.; ×, $U_1/\nu = 1{\cdot}9 \times 10^5$, $y = 0{\cdot}048$ in.

to a localized spanwise variation in boundary-layer Reynolds number, with a resulting localized variation in the amplification rate. This reasoning suggests that the peaks and valleys of the spanwise distribution in wave amplitude for a wave near branch I of the Tollmien–Schlichting stability diagram should be reversed with respect to the peaks and valleys of a wave near branch II. Span-

wise distributions of u' and U are shown in figure 13 for a 65 c/s wave at two different Reynolds numbers per foot. Comparison of the intensity of the 65 c/s wave at a Reynolds number per foot of $3{\cdot}1 \times 10^5$, which lies near branch I, with the intensity of the 145 c/s wave shown in figure 2, which lies near branch II, shows that their peaks and valleys are interchanged. At a Reynolds number per foot of $1{\cdot}9 \times 10^5$, the 65 c/s wave lies near branch II, and the peaks and valleys have again reversed. The spanwise variation in local mean velocity, which is indicative of the existence of the longitudinal eddy system, shifts with the peaks and valleys of the intensity distributions. It is this behaviour relative to a fixed experimental arrangement which warrants the conclusion that the eddy system is not spurious, and that it is an integral part of the non-linear three-dimensional wave motion.

(*a*) *Instability due to concave streamline curvature*

An important question is whether the Görtler–Witting mechanism may be responsible for the existence of the longitudinal eddies. Görtler & Witting (1957) have proposed the concept that the concave streamline curvature associated with the wave motion may generate longitudinal vortices in a manner similar to that prescribed for a concave surface. As shown by Klebanoff & Tidstrom (1959), their criterion for the initiation of vortices involves such small-wave amplitudes that it would be met at the input levels introduced by the vibrating ribbon, thus making a direct experimental check on the onset of such an instability not feasible. However, Görtler & Witting conclude that the vortices should exist only in the immediate vicinity of the troughs of the wave, and it was possible to investigate this experimentally. The manner in which this was done is illustrated by figure 14, plate 2. This shows the u-fluctuation at a peak in the upper half of the figure, and the corresponding w-fluctuation at a neighbouring side in the lower half, for different positions across the boundary layer. The oscillograms shown were obtained at a stage of the wave growth corresponding to station C. The top trace in each oscillogram is the fluctuation of either u or w about its mean value. (When positive, u and w are above the respective mean value.) The second trace is a reference wave which was the input signal to the vibrating ribbon. The fluctuation and the reference wave were observed simultaneously on a dual-beam oscilloscope. The third trace is a calibrating voltage. From the instantaneous variation of the fluctuation from its mean value, together with the calibrating voltage and wire sensitivity, one obtains the instantaneous distribution of the fluctuation across the boundary layer at a given time. This was done for the w-fluctuation at different times covering one cycle of the u-fluctuation. When this is combined with the mean spanwise component to obtain the total spanwise component of velocity, it is possible to determine whether or not the eddy exists where the streamline is concave. The results of such a determination at stations B and C are shown in figures 15 and 16. At the top of each figure is the u-fluctuation at a peak varying in time as calculated from oscillograms obtained at $0{\cdot}13\delta$, and $0{\cdot}11\delta$, for stations B and C, respectively. The values θ indicate the time at which the distributions across the boundary layer of the total spanwise component of velocity were obtained. The distributions shown were obtained at one side of the peak in u' at station B, and at each side of the peak in u' at Station C. The

accuracy of the measurements is rather poor near the outer region of the boundary layer because of the very small changes in flow direction. The distribution at the time $\theta = 0°$ is also not too accurate since it depends on the difference of nearly equal quantities. However, the essential features are clear. It is seen that the eddy does not exist all of the time; it begins to make its appearance at about $\theta = 135°$, is fully developed at $\theta = 180°$, and then disappears. The interesting feature is that it exists when the u-fluctuation at the peak tends to be a minimum,

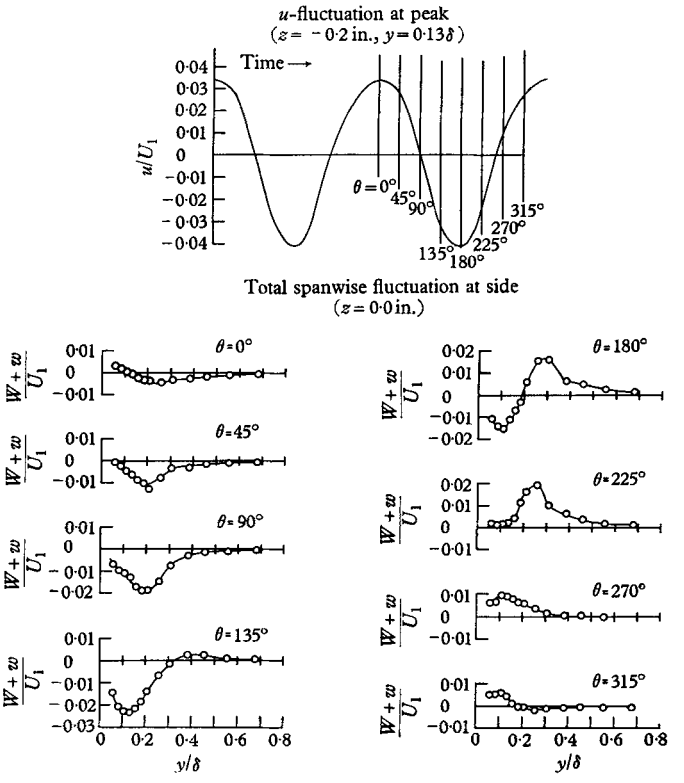

FIGURE 15. Distributions of the total spanwise component of velocity across boundary layer. Station B: 145 c/s wave, $U_1/\nu = 3{\cdot}1 \times 10^5$ ft.$^{-1}$.

or when the streamline tends to be convex rather than concave. Actually, when the wave is concave, for example, at $\theta = 0°$, there is little evidence of any significant eddy system. It is concluded therefore that the Görtler–Witting mechanism does not provide an adequate explanation for the observed behaviour. Although the Görtler–Witting mechanism may be present, it does not play a dominant role in the transition process. The time dependence of the longitudinal eddy system provides a reasonable explanation for the wave forms at peak and valley shown in figure 6, plate 1, and at a peak position in figure 14, plate 2. At a peak the eddy motion brings in low velocity air at a time the velocity fluctuation associated with the wave motion tends to decrease to a minimum. This reinforces the decreasing velocity part of the cycle and is probably the major factor controlling the harmonic content observed at a peak, which has been previously

discussed. However, at about the same time, the eddy motion brings in high velocity air at a valley, which opposes and more than offsets the tendency of the fluctuation to decrease to a minimum with a resulting distortion in wave form.

(*b*) *Vortex-loop concept*

The possibility existed that the observed eddy system might be associated with the x-component of vorticity of a vortex loop. It thus became necessary that an attempt be made to resolve the question as to whether the longitudinal

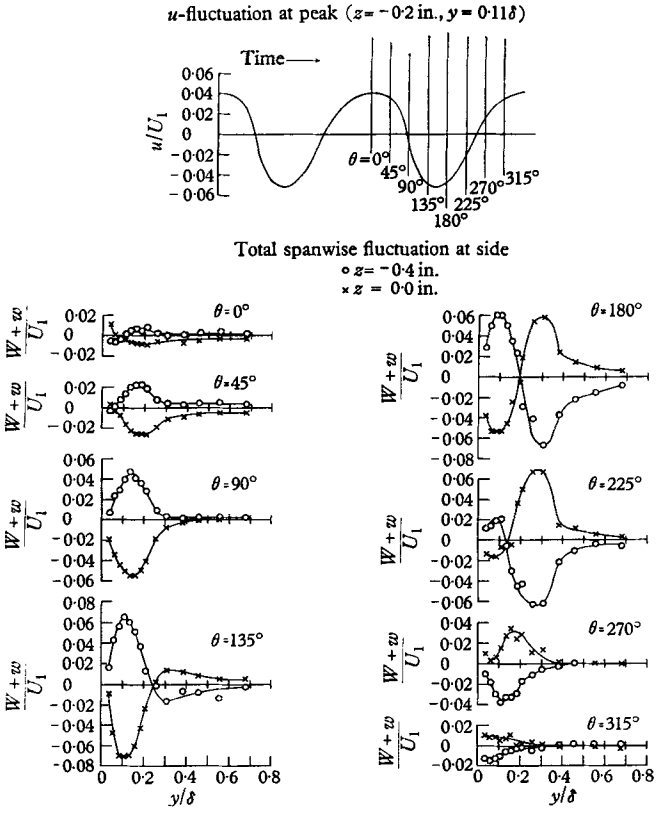

FIGURE 16. Distributions of the total spanwise component of velocity across boundary layer. Station C: 145 c/s wave, $U_1/\nu = 3{\cdot}1 \times 10^5$ ft.$^{-1}$.

vortices could be accounted for by the occurrence of vortex loops such as proposed by Theodorsen (1955), and which have been inferred from visual observations in water on a flat plate behind a trip wire using dye techniques (Hama *et al.* 1957). If such were the case, one would expect that the instantaneous distribution across the boundary layer of the u-fluctuation associated with the z-component of vorticity of the vortex loop would exhibit a phase reversal similar to that shown by the total spanwise component of velocity in figures 15 and 16. Figure 17 shows the distribution of the u-fluctuation across the layer at a side of the peak in u' for stations B and C, and at the time $\theta = 180°$. It is apparent that the u-fluctuation does not undergo the phase reversal which would be expected if the eddy

system arose from a vortex loop formation. Actually the distribution is still markedly similar to the Tollmien–Schlichting distribution. It is therefore concluded that the longitudinal eddy system is not a manifestation of the vortex loop. This conclusion is also supported by the experimental result shown in figure 7, that the phase velocity of the disturbance is still in good agreement with the Tollmien–Schlichting value well into the non-linear range. This is at variance with the experiments behind a trip-wire using dye in water. In these experiments (Hama *et al.* 1957) it was observed that as soon as the looped configuration of the dye line appears, the velocity of the head of the loop increases rapidly as it is carried downstream by the ambient mean velocity. The point of view taken here is that the dye technique marks the fluid particle and therefore shows the

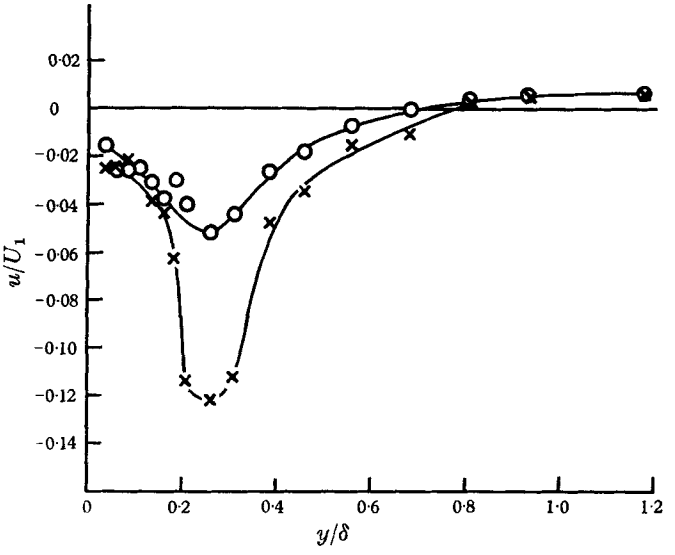

FIGURE 17. Distribution of u-fluctuation across boundary layer at time $\theta = 180°$: 145 c/s wave, $U_1/\nu = 3{\cdot}1 \times 10^5$ ft.$^{-1}$. ○, Station B: $z = 0{\cdot}0$ in., $\theta = 180°$. ×, Station C: $z = 0{\cdot}0$ in., $\theta = 180°$.

behaviour of the mean flow but not necessarily that of the disturbance. It may be speculated that the longitudinal-eddy system which has been described displaces a line of dye in and out from the surface at different spanwise positions, and, as a consequence of the velocity gradient across the layer, a loop configuration is formed. Serious attention should be given to reconciling the opposing points of view arising from this investigation and those relying on fluid markers such as dye or smoke. It is felt that this difference is due to the method of observation and the interpretation of results, and not that the phenomena are basically different. However, the possibility that the phenomena observed in the dye experiments are associated with the eddies which may be shed at some critical Reynolds number for the trip-wire, and are not the Tollmien–Schlichting wave warrants investigation.

(*c*) *Secondary motions induced by non-linear interaction*

In order to gain an insight into what may be the governing mechanism for the observed longitudinal vortices, the growth of the wave was studied with particular emphasis on the conditions for departure from the linear theory. Measurements of the intensity of the u-fluctuation were made in the vicinity of the critical layer at a position corresponding to a peak in the spanwise distribution of wave amplitude. The wavelength of the disturbance was varied from 1·5 to 3·0 in. and the Reynolds number per foot from $1{\cdot}9 \times 10^5$ to $3{\cdot}1 \times 10^5$. The observed intensity at the point of departure from the linear range varied from 1·3 to 2·2% of the free-stream velocity, and no consistent trend with wavelength or Reynolds number per foot was apparent. However, the results did indicate that the departure from the linear theory may be governed by the degree of spanwise irregularity in wave amplitude. This, together with the fact that the wave motion in the non-linear range still retains a semblance of linear behaviour, would suggest that the observed effects may be accounted for by another approximation in a perturbation theory in which three-dimensional non-linear effects are considered.

A theoretical analysis along these lines has recently been made by Benny & & Lin (1960). It should be noted that their analysis was carried out for a mean-velocity profile characteristic of free shear layers rather than the Blasius distribution of the flat-plate boundary layer. However, it is reasonable to expect the gross features to be generally applicable. Benny & Lin considered the non-linear behaviour of a primary oscillation which consists of two components, a two-dimensional Tollmien–Schlichting wave and a superposed three-dimensional wave that has a periodic spanwise variation in wave amplitude. The non-linear interaction of these two modes when the two-dimensional component predominates gives rise to a longitudinal-eddy system in the nature of a secondary flow with the same spanwise wavelength as the primary oscillation. The momentum exchange associated with this secondary flow is in such a direction as to produce a velocity defect at the spanwise positions where the amplitude of the wave is a maximum (peak), and an excess where it is a minimum (valley) with corresponding changes in the mean-velocity profile. Perhaps most significant, there is a time dependence of the eddy system such that the eddy is most intense when the streamline is convex. It is evident that these theoretical conclusions are remarkably consistent with the experimental results that have just been presented.

In a more detailed analysis by Benny (1961), it has been shown that as the three-dimensional component of the primary oscillation becomes more pronounced the original vortices move closer to the peak and much weaker vortices with opposite rotation should begin to appear near the valley; and in the extreme case of a completely dominant three-dimensional component, an eddy system with half the spanwise wavelength will be evolved. This behaviour was also found to be consistent with the experimental findings. Figure 18 shows the measured distributions across the boundary layer of the spanwise mean-velocity component in the region from a peak to a valley at the different downstream

stations B, C, and D of the wave growth. The streamline patterns in the (y, z)-plane inferred from these distributions are shown schematically in figure 19. As mentioned previously, the measurements of W were somewhat inaccurate in the outer regions of the layer. Consequently the stagnation streamlines of the eddy motion could not be obtained, and these are not shown in the figure. In addition the measurements were not made in sufficient detail to construct reliably the streamline pattern of the eddy which develops near the valley at station D, and these streamlines are therefore indicated by dashed lines. One further remark is required. In the Benney–Lin analysis of the free shear layer, there exist counter-rotating eddies on each side of the critical layer. It may well be that the change

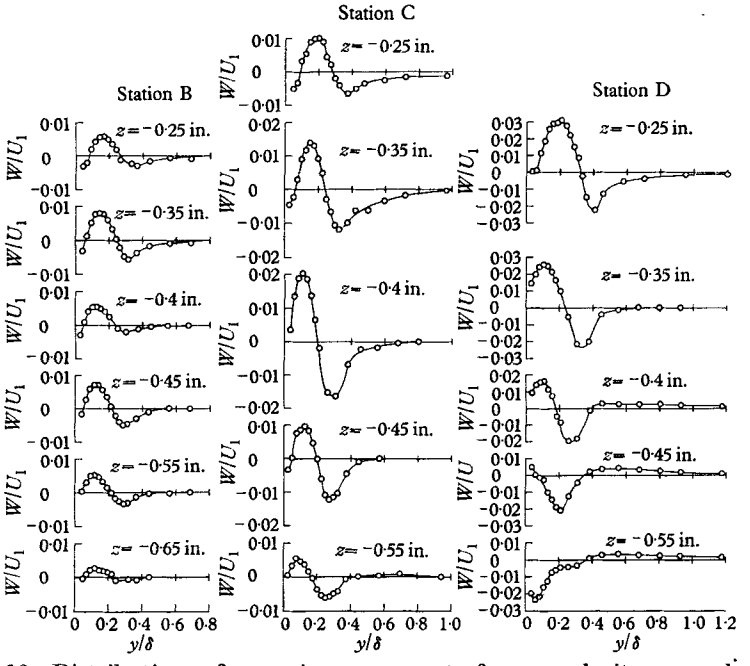

FIGURE 18. Distributions of spanwise component of mean velocity across boundary layer: 145 c/s wave, $U_1/\nu = 3{\cdot}1 \times 10^5$ ft.$^{-1}$.

in sign of W close to the wall shown in the distributions of figure 18 are indicative of a counter-rotating eddy on the wall side of the critical layer which is suppressed by the presence of the wall. In the case of the boundary layer, there are as yet no theoretical guide-lines by which to assess this behaviour. Measurements of W sufficiently close to the wall are difficult; and inasmuch as the magnitude of W is also small, no clear physical interpretation emerges from the experimental data. If such an eddy does exist on the wall side of the critical layer, the streamline patterns shown in figure 19 would have to be modified accordingly, since they were constructed by ignoring the change in sign of W close to the wall.

Apart from these qualifying remarks the essential features are markedly consistent with the Benney–Lin analysis. At station B the longitudinal eddy occupies the region from a peak to a valley, and one would infer that at this position the two-dimensional–three-dimensional interaction is dominant. As

the wave intensifies and the three-dimensional mode becomes more significant, the original vortices intensify and move closer to the peak, and at station D the tendency for the eddy system to halve its wavelength is clearly evident. However, breakdown of the wave occurs before the doubling of the eddy system can become fully developed. This behaviour of the longitudinal eddy system is also reflected in the mean-velocity distributions shown in figure 20. It is also

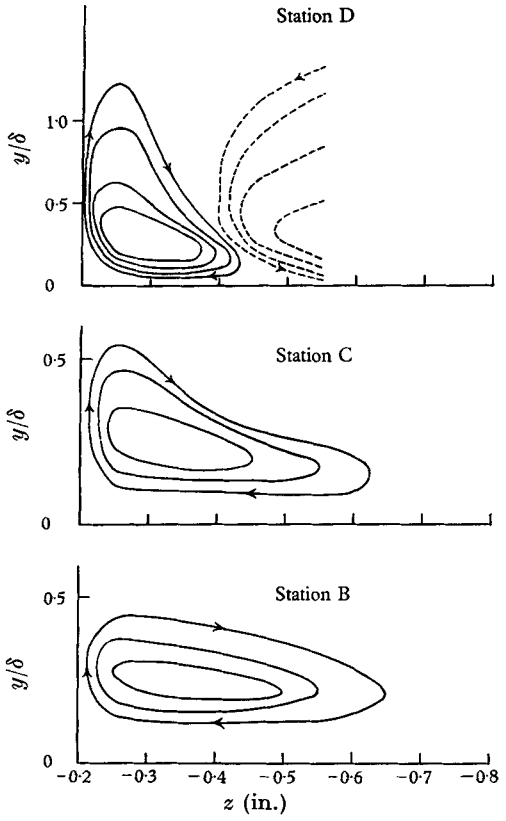

FIGURE 19. Schematic representation of streamlines in (y, z)-plane: 145 c/s wave, $U_1/\nu = 3{\cdot}1 \times 10^5$ ft.$^{-1}$.

consistent with this behaviour for the velocity defect region at a peak to be more pronounced and more concentrated than the region of velocity excess. Benney & Lin in their analysis assume that the two-dimensional and three-dimensional components of the primary oscillation have the same velocity and are therefore locked in phase. On the other hand, Stuart (1960*a*, *b*) has inferred from linear theory and the Squire transformation that the velocities of these two fundamentals may differ by as much as 15 %. Consequently the time-dependent eddy system may undergo a phase shift of 180 degrees within three or four wavelengths, which is about the extent of the region from stations A to D in the present experiment. Measurements of the time-dependent eddy system at stations B and C in figures 15 and 16 show no significant phase shift, i.e. at both positions the eddy is most intense when the streamline is convex. However, the possibility that in the present experiment the velocities of the two fundamental modes do

not differ to the extent cited above cannot be ignored. In addition, the measurements were made over a distance of about one wavelength, and the phase shift if any would be small and not detectable within the experimental accuracy. Although this question is therefore not resolved in a completely satisfactory manner, the present experimental evidence would indicate that the assumption

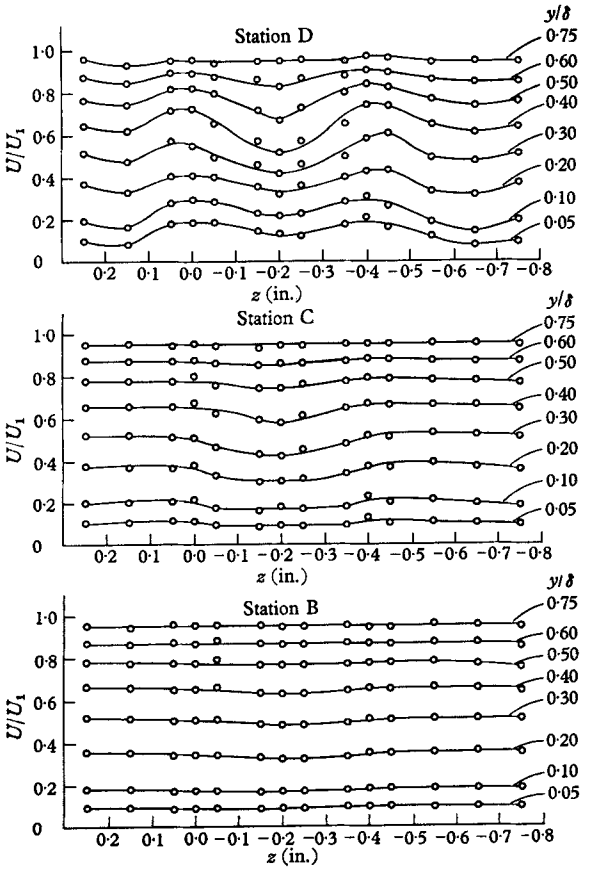

FIGURE 20. Spanwise distributions of mean velocity: 145 c/s wave, $U_1/\nu = 3{\cdot}1 \times 10^5$ ft.$^{-1}$.

of equal wave velocities is a very reasonable one. Although a final evaluation must await the extension of the theory to the Blasius distribution, there is good reason to believe that most of the experimentally observed phenomena will be accounted for by the type of theoretical approach conducted by Benney & Lin. While the theory deals with non-linear effects, it stops short of the actual breakdown process and the onset of turbulence. This part of the process was investigated experimentally and will be discussed in the following section.

5. Mechanism of breakdown

The term breakdown is used herein to describe what appears to be an abrupt change in the character of the wave motion at a peak and the onset of what is believed to be a new instability. Oscillograms which illustrate the nature of the

breakdown process at a peak are shown in figure 21, plate 3. They were obtained for an arbitrary fixed ribbon amplitude at the different distances downstream from the vibrating ribbon noted above each oscillogram, and at 0·12 in. from the surface. This y-position corresponds to about $0{\cdot}6\delta$ at the beginning of breakdown, and is where the breakdown as detected by a hot-wire sensitive to the u-fluctuation is most intense and most easily observable. The top trace in each oscillogram is the u-fluctuation varying in time about its mean value. (Decreasing velocity is in a downward direction.) The second trace is a reference wave which was the input signal to the vibrating ribbon. The fluctuation and the reference wave were observed simultaneously on a dual-beam oscilloscope.

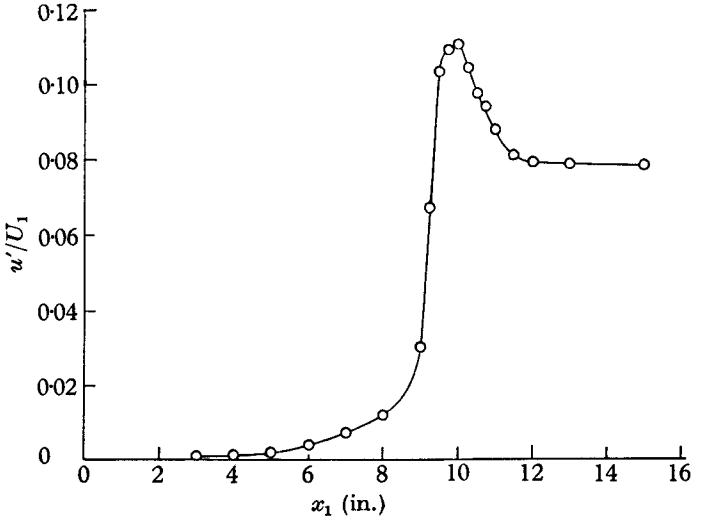

FIGURE 22. Growth in intensity of u-fluctuation associated with the oscillograms of figure 21: 145 c/s wave, $y = 0{\cdot}12$ in., $z = -0{\cdot}2$ in., $U_1/\nu = 3{\cdot}1 \times 10^5$ ft.$^{-1}$.

The breakdown process is characterized by intense fluctuations in the direction of lower velocity which occur for each cycle of the primary wave. They increase in number and form packets of high-frequency fluctuations which follow in succession, and when they have overtaken one wavelength of the primary wave, they have caught up with one another. The amplitude of the fluctuation may be as much as 40 % of the free-stream velocity in the direction of lower velocity. It is the beginning of the single intense fluctuation, as shown in the oscillogram at $x_1 = 9{\cdot}00$ in., which is taken as the position of initial breakdown referred to in the preceding discussion. The abruptness and high intensity with which this phenomenon occurs are characteristic features. As shown by the fluctuation at 1 in. upstream from breakdown, the primary wave is still comparatively free of distortion. The abruptness with which this phenomenon occurs is more graphically illustrated in figure 22, in which the growth in intensity associated with the oscillograms of figure 21, plate 2, is shown. It is seen that there is an almost catastrophic growth in intensity at the position of breakdown, which is indicative of some critical flow condition and the onset of a secondary instability. This point of view is also supported by the similarity of the flow for varying frequencies and

Reynolds numbers per foot. Figures 23 and 24 show the mean velocity and intensity distributions across the boundary layer at the position of initial breakdown for two conditions with different frequencies of the primary wave and Reynolds numbers per foot. The mean velocity distributions are in excellent agreement. The intensity distributions do not show as good an agreement in the outer region of the layer. However, a spot check of the intensity distributions for other frequencies and Reynolds numbers per foot at $y = 0{\cdot}2\delta$ and $y = 0{\cdot}6\delta$ gave results

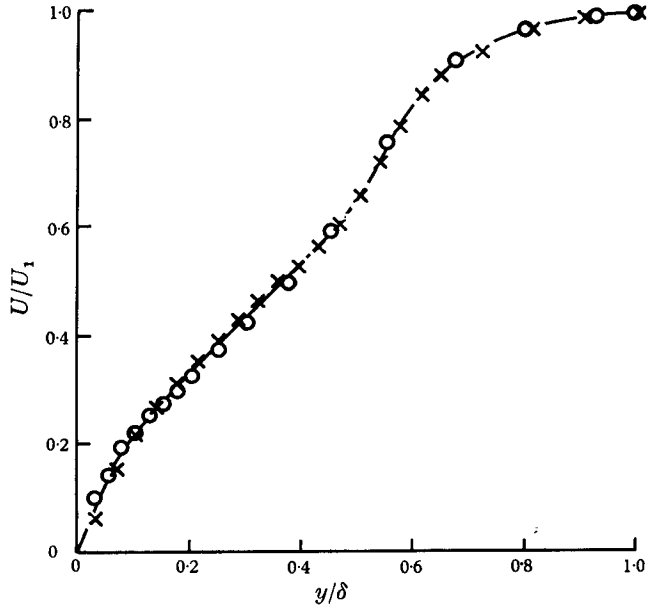

FIGURE 23. Mean velocity distributions across boundary layer at position of initial breakdown for two different wave frequencies and Reynolds numbers per foot. ○, 145 c/s, $U_1/\nu = 3{\cdot}1 \times 10^5$ ft.$^{-1}$; ×, 65 c/s, $U_1/\nu = 1{\cdot}9 \times 10^5$ ft.$^{-1}$.

consistent with the distributions shown. Consequently it is felt that, in view of the very rapid increase in intensity associated with breakdown as shown in figure 22 and the difficulty in being at exactly the same relative stage of the breakdown process, there appears little doubt that the distributions at breakdown are similar and do not depend significantly either on Reynolds number per foot or frequency of the primary wave.

In order to determine the spatial extent of initial breakdown as well as its physical significance, attention was given to the manner in which the high-frequency fluctuations characteristic of breakdown varied in the z- and y-directions. Oscillograms of simultaneous signals from two hot-wires sensitive to the u-fluctuation for the case where the wires were separated in the z-direction, and for another where they were separated in the y-direction, are shown in figures 25 and 26, plates 4 and 5, respectively. The oscillograms in figure 25 show the effect of a variation in the z-direction for two different stages of the breakdown process. The top trace in each of the oscillograms is the signal from a hot-wire probe kept at a fixed spanwise position corresponding to a peak in the spanwise variation of u', and the lower trace is the corresponding signal from a hot-wire probe displaced

different amounts in the z-direction. The positions noted above each oscillogram are the actual spanwise positions. Both hot-wire probes were at 0·12 in. from the surface. The important feature is that after a separation of 0·1 in. the signal from the hot-wire probe which is displaced shows a phase reversal, i.e. the 'spike' is now in the direction of increasing velocity. The amplifier gain settings at which the various traces were obtained were quite arbitrary, and no particular attention should be given to the relative amplitude of the fluctuations in the different oscillograms. However, it can be qualitatively noted that the 'spike' in the direction of higher velocity is less intense than that in the direction of decreasing velocity. At a spanwise separation of 0·35–0·45 in. all indications as to breakdown have disappeared. The oscillograms in figure 26, plate 5, show the simultaneous

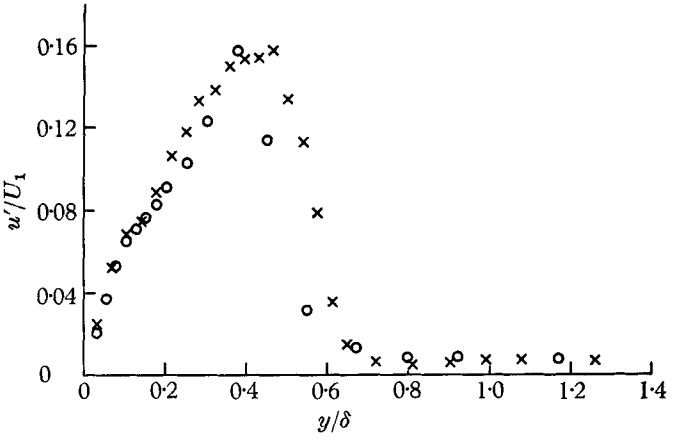

FIGURE 24. Distribution of intensity of u-fluctuation across boundary layer at position of initial breakdown for two different wave frequencies and Reynolds numbers per foot. ○, 145 c/s, $U_1/\nu = 3{\cdot}1 \times 10^5$ ft.$^{-1}$; ×, 65 c/s, $U_1/\nu = 1{\cdot}9 \times 10^5$ ft.$^{-1}$.

signals from two hot-wire probes displaced in the y-direction. Both hot-wire probes were at a spanwise position corresponding to a peak. The top trace in each oscillogram is the signal from the probe kept at $0{\cdot}6\delta$, while the lower trace is from the displaced probe. The positions noted above each oscillogram are the actual positions within the boundary layer. In this case the breakdown makes itself felt across the entire boundary layer. The significant feature is again the phase reversal of the 'spike' which occurs in the outer region of the layer between $0{\cdot}75\delta$ and $0{\cdot}8\delta$. The conclusion to be drawn from the nature of the oscillograms shown in figures 25 and 26 is that the intense high-frequency fluctuations associated with breakdown are the manifestation of the generation of 'hairpin' shaped eddies which rotate in such a manner as to produce an intense low-velocity fluctuation within the loop. The extent of the eddy in the y-direction is somewhat greater than δ, while that in the z-direction, at least in the initial stage of breakdown, is of the order of 4δ. It is seen from the oscillograms in figure 26 that the u-fluctuation in the inner region of the boundary layer only weakly reflects the existence of the eddy. It may be speculated that the reason for this is that the spatial orientation of the eddy is such that, near the surface,

it is the x-component of vorticity which is most intense. In this connexion, observations of the signal from a w-fluctuation probe may prove informative.

The simultaneous traces shown in (*b*) of figure 25, plate 4, for a spanwise variation of 0·1 in. illustrate an interesting feature of the 'hairpin' eddies. Time progression is from left to right. It is seen that the 'spikes' which result from the eddy which first arrives are out of phase. On the other hand, the spikes which result from the eddy which was generated closer to the position of observation and arrives a short time later are in phase. This behaviour is interpreted as signifying that the eddies are stretched as they propagate downstream. The eddies which are formed from one cycle of the primary wave overtake those of the previous cycle, and it is therefore evident that they are travelling faster than the condition which created them. A measure of their velocity was obtained by observing the simultaneous signals from two hot-wires separated 0·51 in. in the downsteam direction with one wire directly behind the other. Interference was avoided by making the upstream wire longer than the downstream wire and by using very fine prongs. Both wires were at a spanwise position corresponding to a peak and at 0·12 in. from the surface. A representative sample of the traces obtained is shown in figure 27, plate 6. It is seen that the eddy arrives first at the upstream wire, and then a short time later on the downstream wire. In the distance between the two wires another eddy has been formed which is detected by the downstream wire. The velocity of propagation in the initial stage of breakdown was determined from the time delay as given by the timing signal, and the average value found from a number of such records was $0{\cdot}68U_1 \pm 0{\cdot}04$. This value did not appear to depend on Reynolds number per foot or frequency of the primary wave.

Since the whole process is typical of an eddy-shedding mechanism as viewed by an observer travelling with the wave velocity, it is desirable to evaluate some of the features which are known to be associated with this type of instability. As shown in figure 21, plate 3, the eddies are quite unstable and very quickly develop into the fluctuations which are typical of turbulent flow. However, in the initial stages of breakdown they have a definite frequency which can readily be determined. This was done for various Reynolds numbers per foot and a number of different frequencies of the primary wave. The results obtained are summarized in table 1, where f_m is the frequency of the 'hairpin' eddy as measured by a stationary observer. The shedding frequency as viewed by an observer travelling with the wave velocity is shown in figure 28 plotted on a log-log basis against the difference between the free-stream and the wave velocity. The wave velocities used are the values listed in table 1, which were measured but are still in the range where good agreement with the linear theory is obtained. There may be, as has been previously pointed out, some increase in wave velocity as breakdown is approached, indicating an acceleration of the fluid mass from which eddies are shed. Neglect of this in figure 28 does not significantly distort the salient features. It is seen that the eddy frequency varies as the $\frac{3}{2}$-power of the relative velocity. A corresponding Strouhal number is shown in figure 29. The number obtained is 0·13, and is independent of Reynolds number when the displacement thickness of the mean velocity profile at breakdown, δ_b^*, is taken as the characteristic length. It should be pointed out that the measurements of δ_b^* were made only

for the two conditions shown in figure 23. However, in these cases the ratio of δ_b^* to the Blasius displacement thickness at breakdown was a constant factor of 1·06, and this factor was used to obtain the remaining values. The eddy-shedding mechanism is remarkably similar in behaviour to that observed in flows that

Primary wave (c/s)	U_1 (ft./sec)	$U_1/\nu \times 10^{-5}$ (ft.$^{-1}$)	c/U_1	f_m (c/s)
40	20·5	1·2	0·36	237
45	41·0	2·5	0·30	654
50	25·4	1·5	0·35	346
65	30·7	1·9	0·34	462
65	51·0	3·1	0·31	1030
105	40·9	2·5	0·35	770
145	52·5	3·1	0·34	1090

TABLE 1

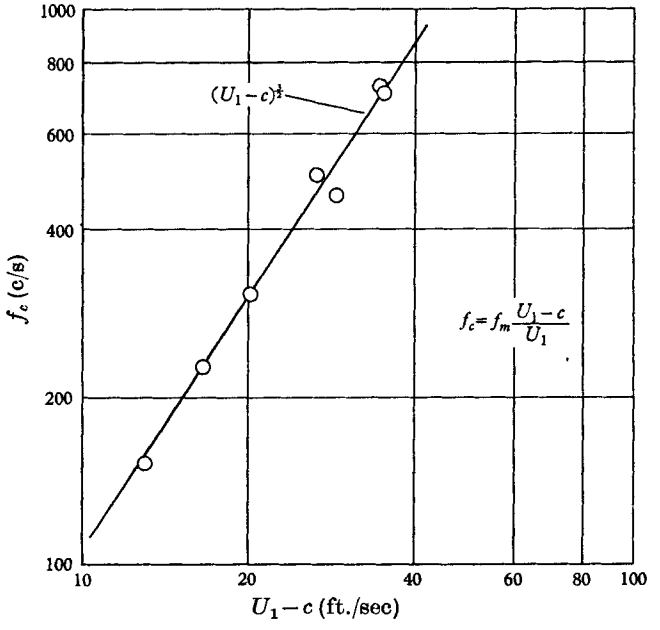

FIGURE 28. Variation of 'hairpin' eddy frequency with free-stream velocity as viewed by an observer travelling with the wave velocity.

undergo inflexional instability such as jets, wakes and the separated layer over a rearward facing step (Sato 1956, 1960). Experimental observations made in such flows, however, do not show the sudden onset of the intense high-frequency fluctuations associated with the 'hairpin' eddies, nor the intermittent turbulent burst of natural transition (Schubauer & Klebanoff 1956). The reason evidently is that in the case of the boundary layer the eddies arise from a secondary instability, while in the inflexional flows the eddies are present from practically the first sign of instability. The possibility of a secondary inflexional instability has

also been suggested by Betchov (1960) from a somewhat different point of view which proposes that it may arise from a large two-dimensional disturbance. It is felt that the results of the present investigation strongly indicate that the three-dimensional non-linear effects are an essential part of the process, not only because of the manner in which they alter the mean-velocity profile, but also because of the effect they have on the growth rate of the wave and the distribution

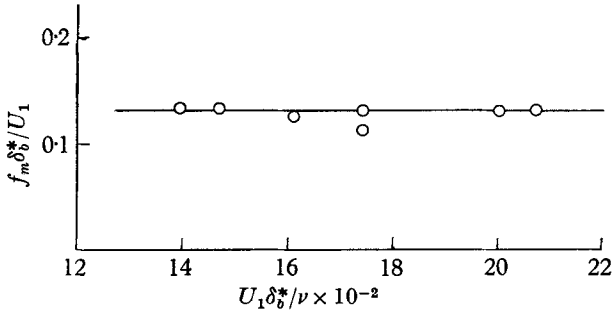

FIGURE 29. Non-dimensional plot of 'hairpin' eddy frequency.

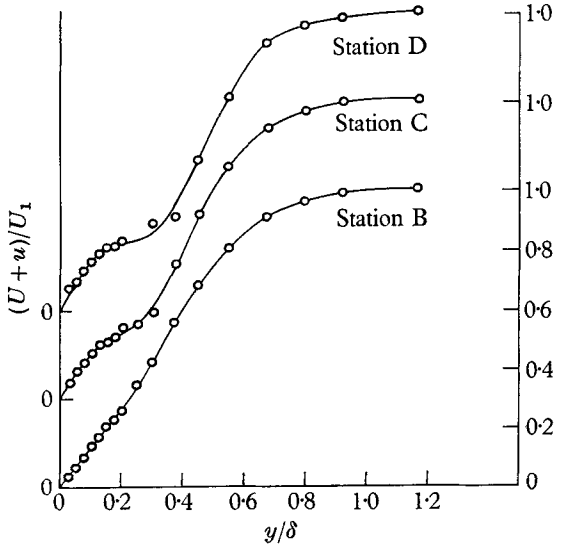

FIGURE 30. Instantaneous velocity distributions across boundary layer: 145 c/s wave, $U_1/\nu = 3{\cdot}1 \times 10^5$ ft.$^{-1}$.

of wave intensity across the layer. Figure 30 shows the distribution across the boundary layer of the instantaneous total longitudinal velocity for the different downstream stations of the non-linear range of the wave growth at a spanwise position corresponding to a peak. In this case the data were corrected for the non-linearity of the hot-wire. The time at which the distributions were obtained was such that the longitudinal fluctuation had decreased to its minimum value at that position from the surface where the intensity as shown in figure 5 is a maximum. It is seen that a very definite inflexional velocity profile has developed at station D. The shedding frequency is relatively high compared to that of the

primary wave, and although the profile shown is an instantaneous one it may be considered to be quasi-steady to an observer travelling with the wave velocity. The qualitative physical picture which emerges is that there is in effect a bulge of displacement thickness which increases as it travels downstream with the wave velocity. It moves slower than the outer flow, and at breakdown a critical flow condition is reached. In this respect the bulge may be considered to be not unlike a three-dimensional roughness element on a wall. Although a limited amount of information exists on the flow over roughness elements (for example, the observations by Kovásznay (1960) of 'hairpin' loops generated by the unsteady flow over a roughness element), a brief study was made to make the comparison somewhat more direct. A hemispherical roughness element 0·063 in. in height was

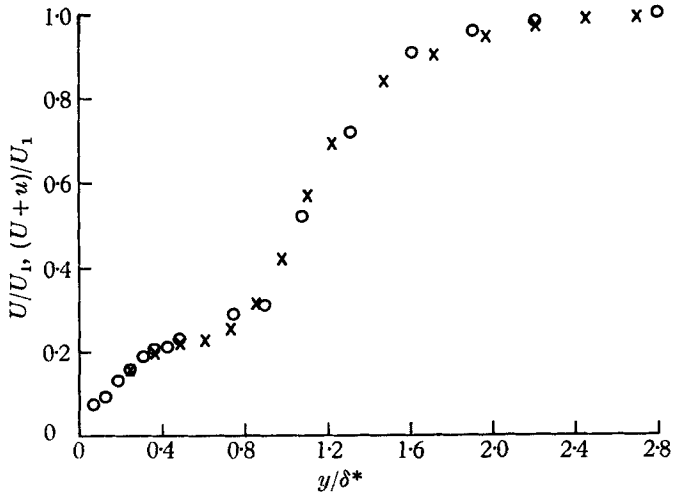

FIGURE 31. Comparison of the instantaneous velocity distribution at wave breakdown with the mean velocity distribution in the unstable region downstream of a roughness element: ○, wave (station D); ×, roughness (hemisphere), k = 0·063 in., x_k = 2·0 ft. (critical), U_1 = 27·0 ft./sec, $x - x_k$ = 1·0 in.

cemented to the surface at 2 ft. from the leading edge of the plate. It was observed that at a critical value of the free-stream velocity, an instability occurred which was characterized by the formation of eddies. In this connexion it is of interest to note that the eddies were not shed directly from the surface of the roughness element, but were first observed downstream of the roughness at a distance of about four times the height. The mean velocity distribution measured 1 in. downstream from the roughness element, at the critical free-stream velocity of 27 ft./sec, is compared in figure 31 with the instantaneous velocity profile obtained at station D. The agreement is striking. The similarity alone does not necessarily provide an insight as to the critical parameters involved in this type of instability. This aspect must await a better understanding of inflexional instability in general. The purpose here is to demonstrate that the inflexional profile associated with the wave motion can undergo the type of instability described.

6. Natural transition

The model of boundary-layer instability which has evolved has come from studies made with a wave artificially introduced by a vibrating ribbon. It was therefore deemed desirable to examine whether the same mechanism applies to the condition of natural transition, i.e. a transition without artificial excitation which is initiated by ambient disturbances such as exist in a wind tunnel. Although this is somewhat more difficult, the previous studies made under controlled conditions have provided several criteria by which a complete identification can be made.

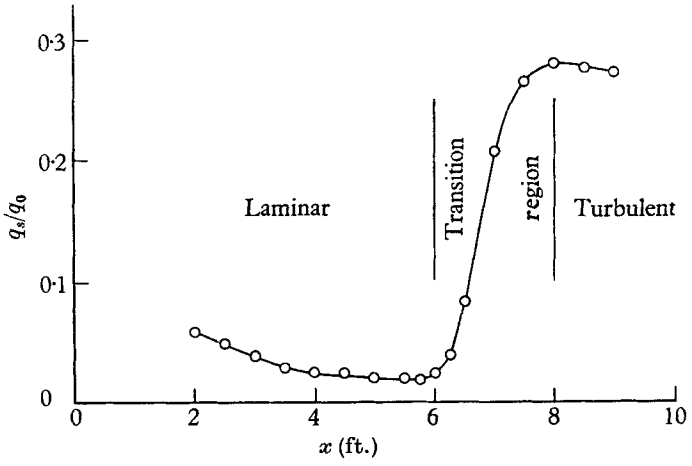

FIGURE 32. Variation of dynamic pressure through a 'natural' transition region as measured with a surface tube: $U_1/\nu = 4{\cdot}6 \times 10^5$ ft.$^{-1}$.

Figure 32 shows the transition region on the flat plate for a Reynolds number per foot of $4{\cdot}6 \times 10^5$. The measurements were made by the conventional method using a surface tube; q_s is the dynamic pressure in the boundary layer measured by the surface tube, and q_0 is the dynamic pressure upstream of the flat plate. The beginning of the transition region corresponds to an x-based Reynolds number of $2{\cdot}8 \times 10^6$, and here transition results from the growth of highly modulated laminar boundary-layer oscillations. The observed frequency of the oscillations leading to transition is 170 c/s, and as usual this falls near branch II of the Tollmien–Schlichting stability diagram. Transition is not well fixed, and the transition region is of relatively long extent compared to the extent in the controlled case.

Spanwise distributions of the wave intensity at 5·5 and 5·75 ft. from the leading edge and 0·052 in. from the surface are shown in figure 33. Under ideal flow conditions with transition arising from purely random disturbances, one would expect that the phenomena which were presented for the controlled case would occur in time at all spanwise positions, and no spanwise variation in wave intensity would be observed. However, it is not at all surprising that spanwise variations are present. Any fixed irregularity sufficiently small not to be detectable within the experimental accuracy may still, on the average, position the

peaks and valleys. In fact, it was observed during the early phase of the study with the controlled disturbance, before the spacers beneath the vibrating ribbon were introduced, that a 1 % spanwise irregularity in the mean flow introduced by a nick in the leading edge of the flat plate had a very strong effect in establishing a peak and valley with an earlier breakdown to turbulent flow than would otherwise occur. A significant question which remains to be answered is whether there is a preferred or 'natural' spanwise periodicity.

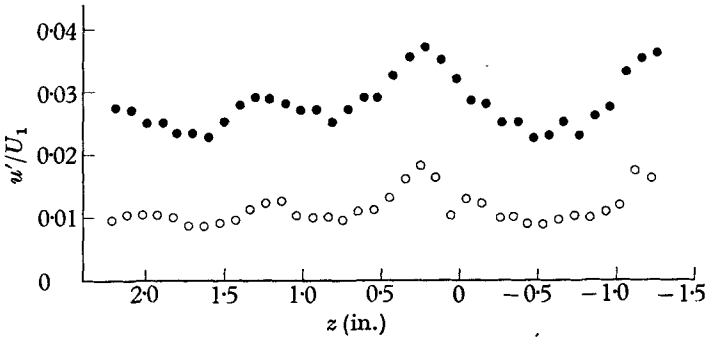

FIGURE 33. Spanwise distributions of intensity of u-fluctuation for 'natural' transition: $y = 0{\cdot}052$ in., $U_1/\nu = 4{\cdot}6 \times 10^5$ ft.$^{-1}$. ○, 5·5 ft. from leading edge; ●, 5·75 ft. from leading edge.

The distributions of wave intensity across the boundary layer at 5·5 and 5·75 ft. from the leading edge are shown in figure 34, and the general features are consistent with what would be expected from the results obtained using the vibrating ribbon. On the average there exists a characteristic difference between peak and valley, with the position of the maximum moving out from the surface as transition is approached. Figure 35 shows the distributions of the mean spanwise velocity component at $x = 5{\cdot}75$ ft. and at $y = 0{\cdot}1\delta$ and $0{\cdot}3\delta$. As in the case of figure 11, the arrows indicating flow direction were arbitrarily changed on the right side of the peak in u'. Such measurements are difficult and their accuracy is low, but they do indicate the generation of a longitudinal-eddy system. The values of W/U_1 are low, as would be expected since they were measurable only because of the positioning of the peaks and valleys on the average. It is stressed that this eddy is not due to any pre-existing irregularity but is generated by the non-linear behaviour of the wave previously described. No such eddy could be detected further upstream. In addition the dominant boundary-layer oscillation lies near branch II of the stability diagram. Consequently, as demonstrated by Klebanoff & Tidstrom (1959), any weak longitudinal eddy, which may not be detectable but may still pre-exist in the mean flow and which would play a role in establishing the peaks and valleys, would rotate in the opposite direction from that shown.

The remaining criterion used to evaluate the similarity between natural and controlled transition is that dealing with the eddy-shedding mechanism which should accompany the breakdown of the wave motion preceding the onset of turbulence. Various aspects of the breakdown process as observed at an x-posi-

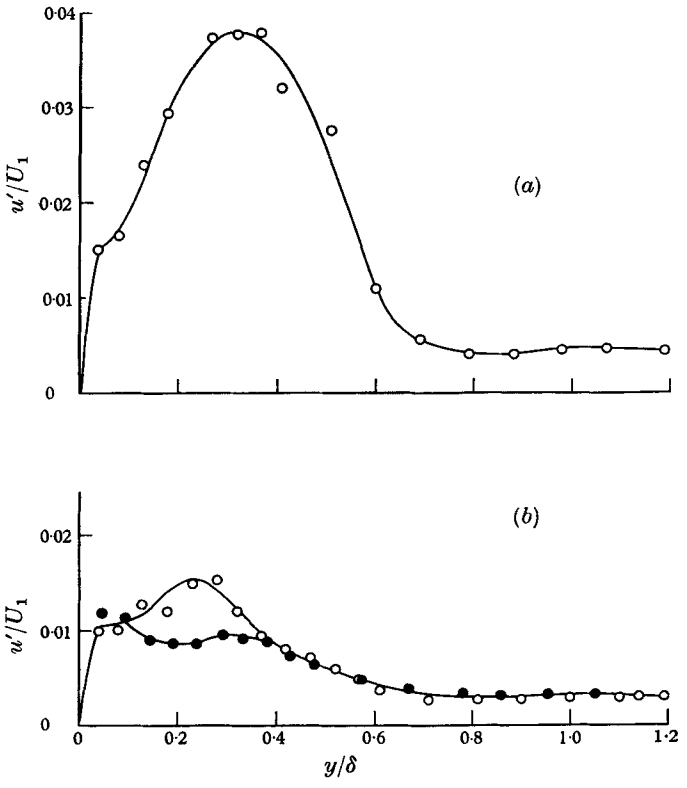

FIGURE 34. Distribution of intensity of u-fluctuation across boundary layer for 'natural' transition: $U_1/\nu = 4{\cdot}6 \times 10^5$ ft.$^{-1}$. (*a*) 5·75 ft. from leading edge: ○, $z = 0{\cdot}25$ in.; (*b*) 5·5 ft. from leading edge: ○, $z = 0{\cdot}25$ in.; ●, $z = -0{\cdot}5$ in.

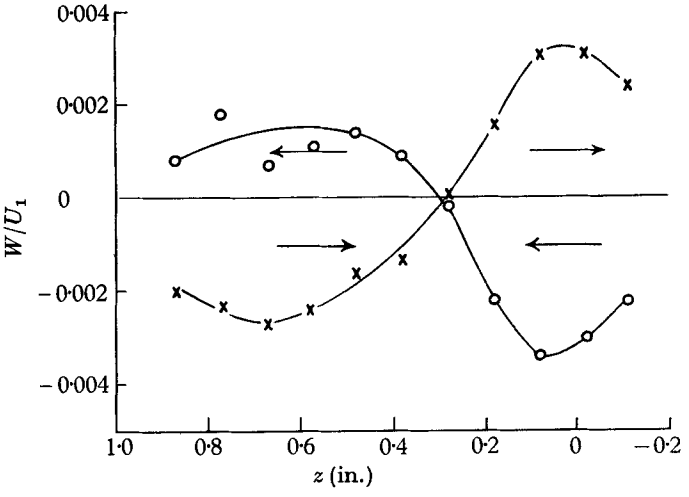

FIGURE 35. Spanwise distribution of spanwise component of mean velocity for 'natural' transition: $U_1/\nu = 4{\cdot}6 \times 10^5$ ft.$^{-1}$. 5·75 ft. from leading edge: ○, $0{\cdot}3\delta$; ×, $0{\cdot}1\delta$.

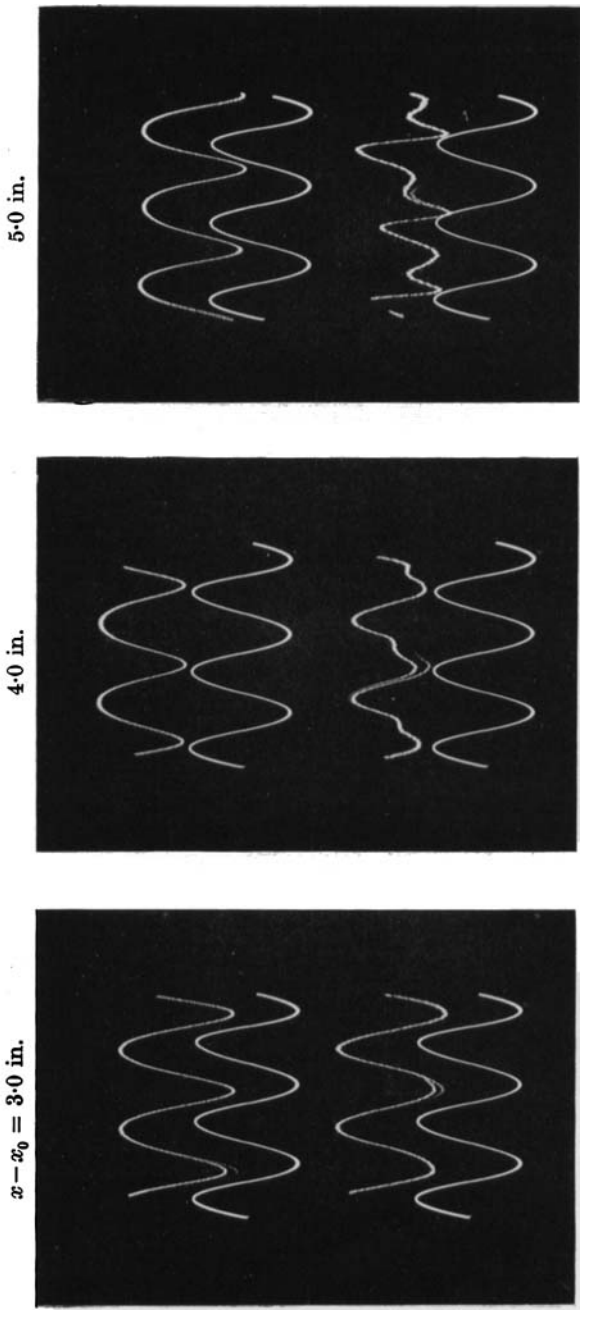

FIGURE 6. Oscillograms illustrating wave-form of u-fluctuation at peak and valley: 145 c/s wave, $y = 0{\cdot}045$ in., $U_1/\nu = 3{\cdot}1 \times 10^5$ ft.$^{-1}$. Time increasing from left to right. Reference signal 145 c/s, decreasing velocity in downward direction. Top trace—peak ($z = -0{\cdot}2$ in.); second trace—reference signal; third trace—valley ($z = -0{\cdot}75$ in.); fourth trace—reference signal.

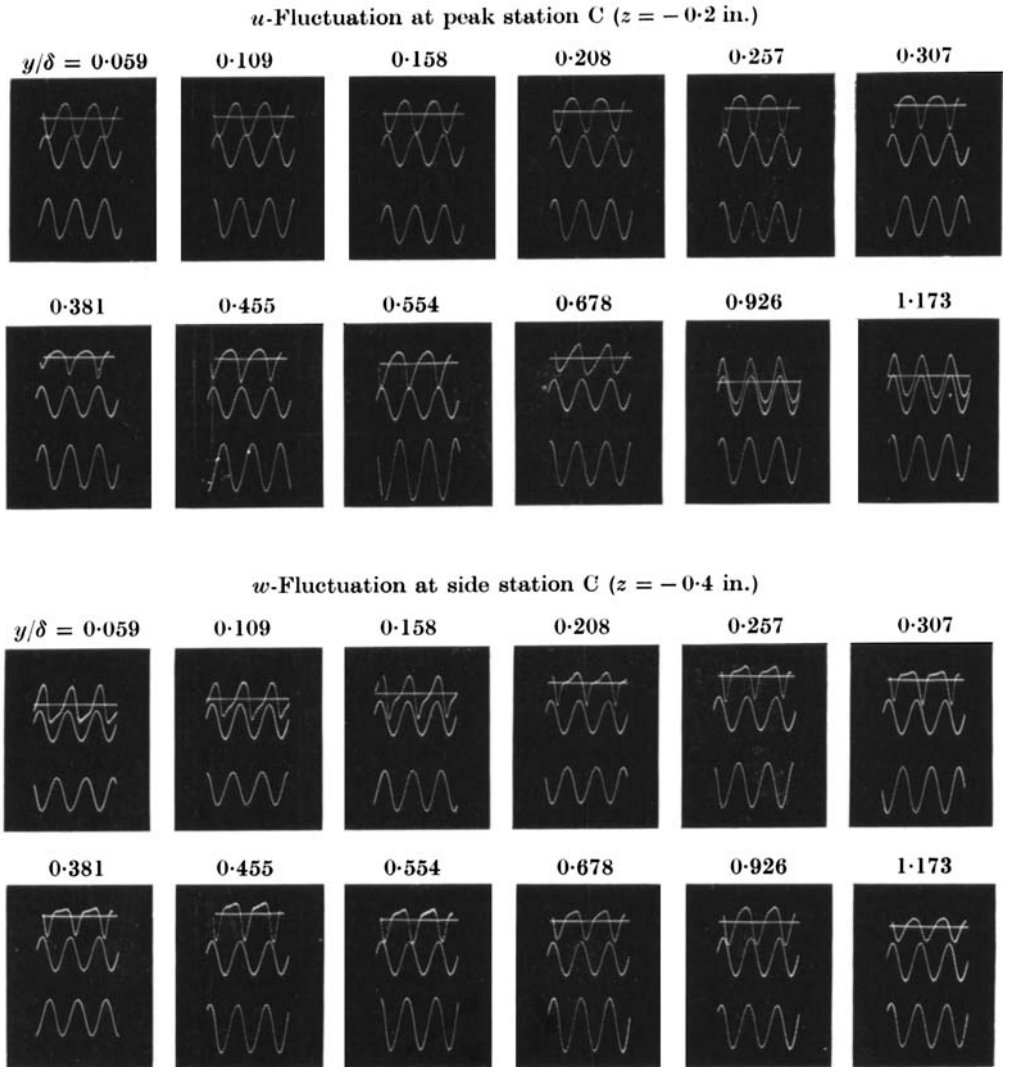

FIGURE 14. Oscillograms of u-fluctuation and w-fluctuation: 145 c/s wave; time increasing from left to right, decreasing velocity in downward direction.

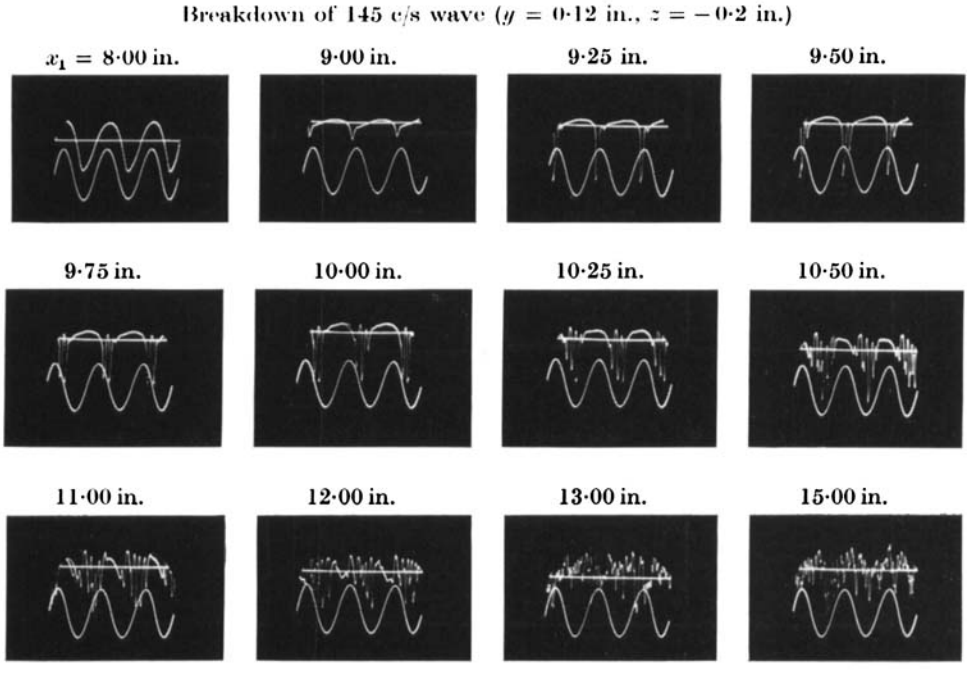

FIGURE 21. Oscillograms of u-fluctuation illustrating breakdown process; time increasing from left to right, decreasing velocity in downward direction; $U_1/\nu = 3{\cdot}1 \times 10^5$ ft.$^{-1}$.

(*a*) Initial stage of breakdown process

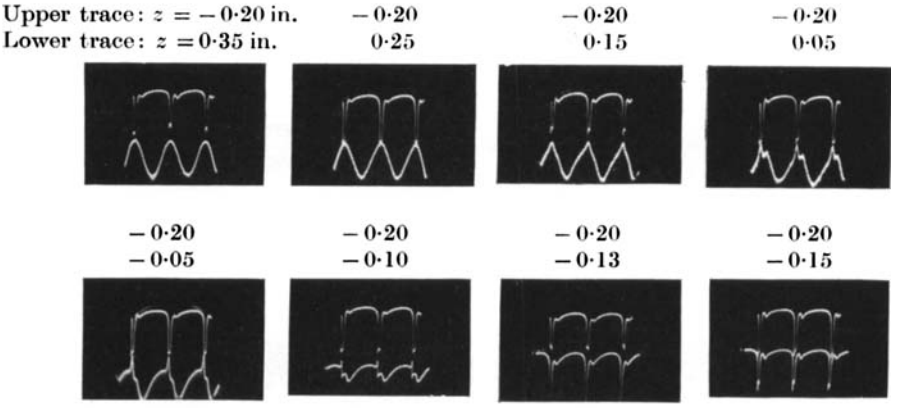

(*b*) A later stage of breakdown process

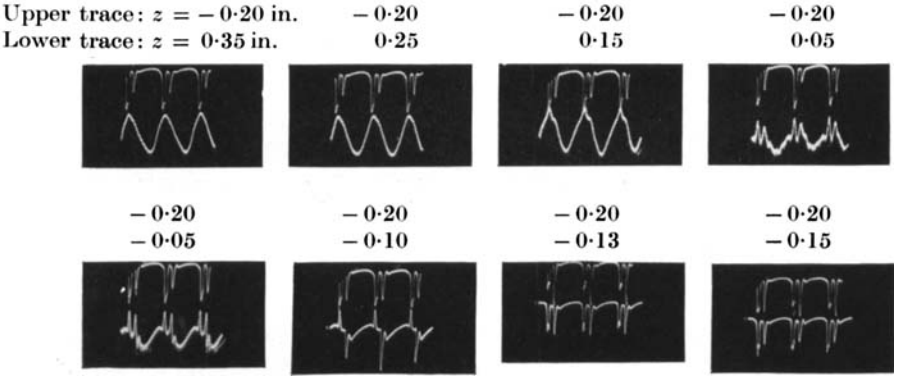

FIGURE 25. Oscillograms of simultaneous u-fluctuations illustrating phase and extent of breakdown in z-direction: primary wave 145 c/s; time increasing from left to right, decreasing velocity in downward direction; $U_1/\nu = 3{\cdot}1 \times 10^5$ ft.$^{-1}$.

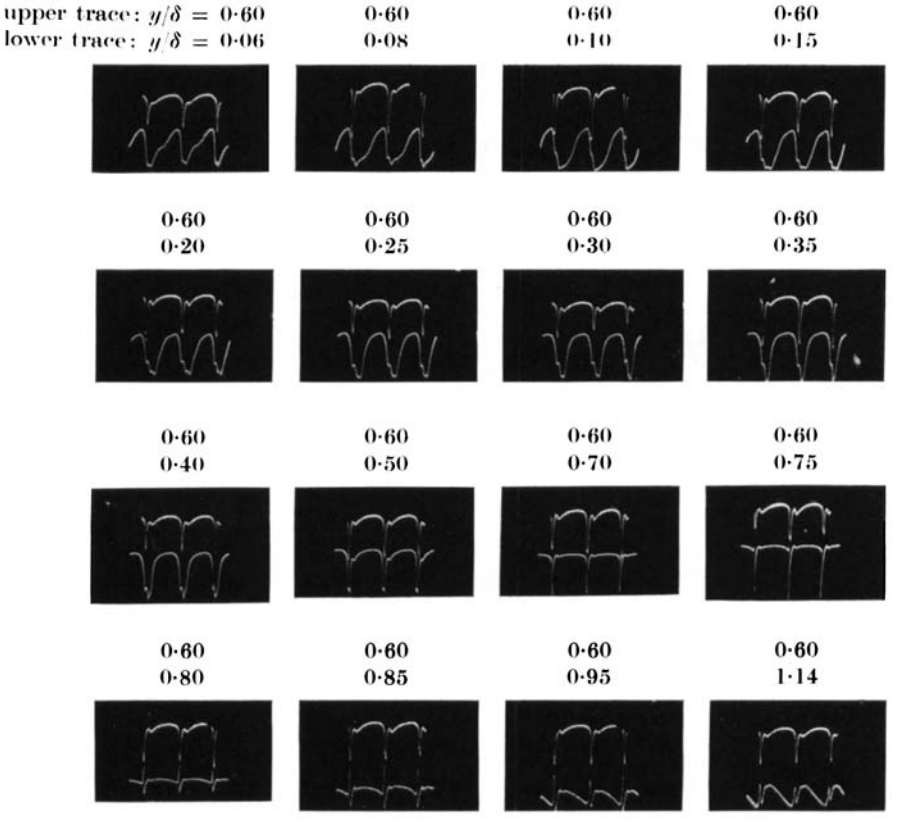

FIGURE 26. Oscillograms of simultaneous u-fluctuations illustrating phase and extent of breakdown in y-direction: primary wave 145 c/s; time increasing from left to right, decreasing velocity in downward direction; $U_1/\nu = 3{\cdot}1 \times 10^5$ ft.$^{-1}$.

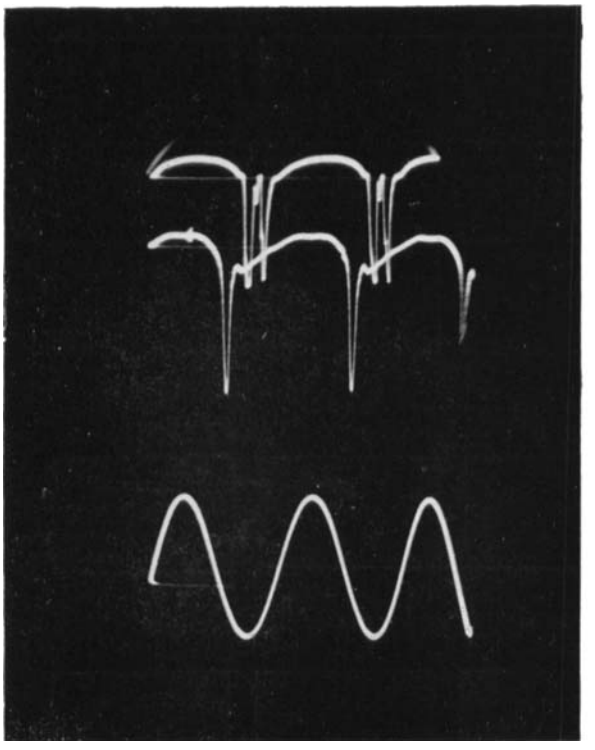

FIGURE 27. Oscillogram illustrating velocity of 'hairpin' eddy: primary wave 145 c/s; time increasing from left to right, decreasing velocity in downward direction;

$$U_1/\nu = 3{\cdot}1 \times 10^5 \text{ ft.}^{-1}.$$

FIGURE 36. Oscillograms illustrating various aspects of breakdown process in 'natural' transition: $U_1/\nu = 4{\cdot}6 \times 10^5$ ft.$^{-1}$; time increasing from left to right, decreasing velocity in downward direction.

tion corresponding to the beginning of the transition region are illustrated by the oscillograms in figure 36, plate 7. These demonstrate the occurrence of the same patterns of intense high frequency fluctuations which are associated with the 'hairpin' eddies. The 'spikes' which now occur intermittently rather than continuously were observed at all spanwise positions, but were somewhat more numerous at the spanwise position corresponding to the peak in u'. The observations were therefore greatly facilitated by positioning the hot-wire at the peak in u'. In order to record the phenomena when they occurred, the 'spike' was used as the trigger for the oscilloscope sweep. The oscillogram labelled (a) is a representative record of two simultaneous signals from two hot-wires displaced in the x-direction which were used for determining the velocity of the 'hairpin' eddy. The short vertical lines in the oscillogram denote a time interval of 1 msec. The velocity of propagation and the shedding frequency observed in the case of natural transition were consistent with the data obtained with the controlled disturbance. The phase relations of the intense high-frequency fluctuations in the y- and z-directions were obtained in exactly the same manner as for the controlled disturbance, and are illustrated by the oscillograms labelled (b) and (c), respectively. It is of interest to note that the oscillogram for a separation of the two hot-wires of $0{\cdot}32\delta$ shows that the eddy which was generated further upstream is in phase, while that generated closer to the hot-wire is out of phase, indicating the tendency of the head of the eddy to lift away from the surface. It would thus appear that not only is there a possibility of the condition responsible for the eddy shedding accelerating, but that the 'hairpin' eddy is also accelerating as it stretches and propagates downstream with the ambient velocity. It is seen that the same phase relaxations exist in natural transition as for the controlled disturbance. It is therefore concluded that the same basic mechanism which has been presented in some detail for a disturbance artificially introduced by the vibrating ribbon is equally applicable to the case of natural transition.

The authors wish to express their gratitude to Dr G. B. Schubauer for many valuable discussions and for his interest and support during this investigation.

REFERENCES

BENNEY, D. J. 1961 A non-linear theory for oscillations in a parallel flow. *J. Fluid Mech.* **10**, 209.

BENNEY, D. J. & LIN, C. C. 1960 On the secondary motion induced by oscillations in a shear flow. *Phys. Fluids*, **4**, 656.

BETCHOV, R. 1960 On the mechanism of turbulent transition. *Phys. Fluids*, **3**, 1026.

EMMONS, H. W. 1951 The laminar-turbulent transition in a boundary layer. *J. Aero. Sci.* **18**, 490.

FALES, E. N. 1955 A new laboratory technique for investigation of the origin of fluid turbulence. *J. Franklin Inst.* **259**, 491.

GÖRTLER, H. & WITTING, H. 1957 Theorie der sekundären instabilität der laminaren grenzschichten. *Boundary Layer Research Symposium, Freiburg* (Ed. H. Görtler), p. 110. Berlin: Springer-Verlag.

HAMA, F. R., LONG, J. D. & HEGARTY, J. C. 1957 On transition from laminar to turbulent flow. *J. Appl. Phys.* **28**, 388.

KLEBANOFF, P. S. & TIDSTROM, K. D. 1959 Evolution of amplified waves leading to transition in a boundary layer with zero pressure gradient. *N.A.S.A. Tech. note*, no. D-195.

KOVÁSZNAY, L. S. G. 1960 A new look at transition. *Aeronautics and Astronautics*, p. 161. London: Pergamon.

LIN, C. C. 1957 On the instability of laminar flow and its transition to turbulence. *Boundary Layer Research Symposium, Freiburg* (Ed. H. Görtler), p. 144. Berlin: Springer-Verlag.

MEKSYN, D. & STUART, J. T. 1951 Stability of viscous motion between parallel planes for finite disturbances. *Proc. Roy. Soc.* A, **208**, 517.

SATO, H. 1956 Experimental investigation on the transition of laminar separated flow. *J. Phys. Soc. Japan*, **11**, 702.

SATO, H. 1960 The stability and transition of a two-dimensional jet. *J. Fluid Mech.* **7**, 53.

SCHUBAUER, G. B. 1957 Mechanism of transition at subsonic speeds. *Boundary Layer Research Symposium, Freiburg* (Ed. H. Görtler), p. 85. Berlin: Springer-Verlag.

SCHUBAUER, G. B. & KLEBANOFF, P. S. 1956 Contributions on the mechanics of boundary layer transition. *N.A.C.A. Rep.* no. 1289.

SCHUBAUER, G. B. & SKRAMSTAD, H. K. 1948 Laminar boundary layer oscillations on a flat plate. *N.A.C.A. Rep.* no. 909.

SPANGENBERG, W. G. & ROWLAND, W. R. 1960 Optical study of boundary layer transition processes in a supersonic air stream. *Phys. Fluids*, **3**, 667.

STUART, J. T. 1958 On the non-linear mechanics of hydrodynamic stability. *J. Fluid Mech.* **4**, 1.

STUART, J. T. 1960*a* Non-linear effects in hydrodynamic stability. *10th Internat. Cong. Appl. Mech., Stresa.*

STUART, J. T. 1960*b* On three-dimensional non-linear effects in the stability of parallel flows. *2nd Internat. Cong. I.C.A.S., Zürich.*

THEODORSEN, T. 1955 The structure of turbulence. 50 *Jahre Grenzschichtforschung* (Ed. H. Görtler & W. Tollmien), p. 55. Braunschweig: Veiweg und Sohn.

WESKE, J. R. 1957 Experimental study of detail phenomena of transition in boundary layers. *Univ. of Maryland Tech. Note*, no. BN-91.